UC San Diego
Other Scholarly Work

Title
Large Scale Air-Sea Interactions with a Simple General Circulation Module; Equilibrium Statistical Mechanics of Quasi-geostrophic Flows

Permalink
https://escholarship.org/uc/item/0fw7t91p

Author
Salmon, Richard L

Publication Date
1976

Peer reviewed

ECKART DISSERTATION PRIZE

The Eckart Dissertation Prize commemorates the late Dr. Carl Eckart; it was first offered in 1975.

Dr. Eckart was a pioneer in the field of quantum mechanics and underwater acoustics, and he served as Director of Scripps Institution of Oceanography from 1948 to 1950. A professor of geophysics from 1948 to 1973, he also established Scripps's Marine physical Laboratory in 1946 and served as its director for two years. He was the first vice-chancellor for academic affairs (1965-66) of the University of California, San Diego, and chaired the university's academic senate for two years (1963-65).

Dr. Eckart was a member of the National Academy of Sciences, American Physical Society, American Geophysical Union, Acoustical Society of America, American Academy of Arts and Sciences, American Association for the Advancement of Science, and other prestigious societies. He received numerous medals and honors, and published more than 70 scientific articles in American and foreign journals during his 71-year lifetime.

The Eckart prize was established by Scripps Director Dr. William Nierenberg and Dr. Joseph R. Curray, then Chairman of the Graduate Department of the Institution, and carries with it a $1,000 award for the "most original and most stimulating" dissertation, presented with coherence, brevity, and clarity.

The prize has a three-fold purpose: to honor the memory of Dr. Eckart, to recognize students who prepare outstanding theses, and to provide a learning experience for students who serve on the selection committee. The committee is composed of one graduate student from each of the seven curricular groups and a faculty member chosen by the chairman of the Graduate Department.

Committee members selecting the second recipient of the Eckart Prize were Duncan C. Agnew, William C. Bartram, R. David Bowlus, George Halikas, Julian P. McCreary, Russell E. McDuff and Carrel A. Ramsey, students, and Professor John D. Isaacs, faculty advisor.

UNIVERSITY OF CALIFORNIA

San Diego

Large Scale Air-Sea Interactions with a

Simple General Circulation Model

and

The Equilibrium Statistical Mechanics of

Quasi-geostrophic Flows

A dissertation submitted in partial satisfaction of

the requirements for the degree of Doctor of Philosophy

in Oceanography

by

Richard Lawrence Salmon

Committee in charge:

Professor Myrl C. Hendershott, Chairman
Professor Charles S. Cox
Professor Russ E. Davis
Professor Daniel B. Olfe
Professor William B. Thompson

1976

The dissertation of Richard Lawrence Salmon is approved,
and it is acceptable in quality and form for publication
on microfilm:

Charles Cox

Russ E. Davis

Daniel B. Olfe

W. B. Thompson.

M C Hendershott
                                    Committee Chairman

University of California, San Diego

1976

DEDICATION

To Mom and Dad

and

Susie and Dee

iii

TABLE OF CONTENTS

Page

LIST OF SYMBOLS

Chapter 1

A	available potential energy
C_p	heat capacity
D	depth of oceanic mixed layer
f	Coriolis parameter
E	eddy viscosity
F	a friction term
H	a heating term
K	kinetic energy
p	pressure
S	Significance parameter
T	averaging time
T_A	deterministic predictability time scale in the atmosphere
T_0	predictability time scale in the ocean
T_s	significance time
V(t)	a general functional of the state of the atmosphere
w	vertical velocity
Y_n^m	a spherical harmonic
$\propto$	colatitude
θ	potential temperature
λ	Newtonian heat exchange coefficient
σ	static stability, a standard deviation
τ	shear stream function

vi

ξ velocity potential

φ longitude

φ_o reference longitude of the maximum anomaly

χ vertical average of the velocity potential

ψ average stream function

Ω angular velocity of the earth

ω vertical velocity in pressure coordinates

Chapter 2

D	mean layer depth
E	energy
f	a general phase function
f_o	Coriolis parameter
h	bottom topography
$J(\ ,\ )$	Jacobian operator
k_i	wavenumber of mode i
k_{def}	reciprocal of the radius of deformation
L_{box}	length of the square model ocean
P	a general point in phase space
$\mathcal{P}$	probability distribution function
r	nondimensional square wavenumber
U,u	conjugate functions
V	a general volume in phase space
x_i, a_i, b_i, A_i, B_i	phase coordinates
Z	enstrophy or potential enstrophy
$\alpha, \beta, \beta_1, \beta_2$	inverse temperatures
β^*	spatial derivative of rotation rate
Γ	phase space
δ	ratio of mean depths
γ	vorticity or potential vorticity
ρ	correlation coefficient
σ	standard deviation
φ_i	an orthonormal eigenfunction

ψ streamfunction

Ω, ω structure functions

$\overline{}$ area integration

LIST OF FIGURES

Chapter 2

LIST OF TABLES

Chapter 1

Chapter 2

ACKNOWLEDGEMENTS

VITA

May 4, 1949 -- Born -- Waukegan, Illinois

1971	B.S. in Meteorology and Oceanography University of Michigan, Ann Arbor
1971 - 1974	NDEA fellow,Scripps Institution of Oceanography University of California, San Diego
1974 - 1975	Research Assistant, Scripps Institution of Oceanography University of California, San Diego

FIELDS OF STUDY

Major Field: Oceanography

Studies in Physical Oceanography and Fluid Mechanics.
Professors Robert S. Arthur, Charles S. Cox,
Russ E. Davis, Myrl C. Hendershott, Walter H. Munk,
Joseph L. Reid, Albert W. Green and Stanley J. Jacobs.

Studies in Meteorology.
Professors Edward S. Epstein and William R. Kuhn.

Studies in Applied Mathematics.
Professors Forman A. Williams and John W. Miles

Studies in Data Analysis and Inverse Theory.
Professors Richard A. Haubrich and Robert L. Parker

Studies in Marine Chemistry.
Professor Joris M. Gieskes

Studies in Marine Biology
Professors John A. McGowan and Michael M. Mullin

Studies in Marine Geology
Professor Henry W. Menard

ABSTRACT OF THE DISSERTATION

Large Scale Air-Sea Interactions with a

Simple General Circulation Model

and

The Equilibrium Statistical Mechanics of

Quasi-geostrophic Flows

by

Richard Lawrence Salmon

Doctor of Philosophy in Oceanography

University of California, San Diego, 1976

Professor Myrl C. Hendershott, Chairman

Two loosely related studies utilize the quasi-geostrophic dynamical equations in applications in which the nonlinear or turbulent terms are of critical importance. In both cases, the importance of the nonlinear terms requires that the solutions to the equations be subjected to a statistical interpretation.

In Chapter 1, I have coupled Lorenz's (1960) two-layer atmospheric model to a "copper plate" ocean to obtain a simple model that can be used to study the effects of large scale sea surface temperature anomalies on the dynamics of the atmosphere. With 164 degrees of freedom, the atmospheric model mimics the observed northern hemisphere

energy cycle in fair detail. In three experiments, each lasting one year, I consider an ocean

     (a) with fixed temperature that depends only on latitude;

     (b) with fixed large amplitude sea surface temperature anomalies; and

     (c) with temperature determined by heat exchange with the air.

The results suggest that, even in the case (b) of exaggerated anomalous forcing where a statistically averaged atmospheric response is detectable, the response may be small compared to random differences that occur in an averaging time as short as one year.

In Chapter 2, I apply the principles of classical equilibrium statistical mechanics to derive the equilibrium states toward which spectrally truncated representations of the equations of motion would evolve in the absence of forcing and viscosity. In the case of two immiscible layers, I find that the internal radius of deformation constitutes an important dividing scale: At scales of motion larger than the radius of deformation, the equilibrium flow is nearly barotropic while at smaller scales the streamfunctions in the two layers are statistically uncorrelated. The equilibrium lower layer flow is positively correlated with bottom topography (anticyclonic flow over seamounts) and the correlation extends to the upper layer at scales larger than the radius of deformation. I suggest that some of the trends observed in non-equilibrium flows may be looked on as manifestations of the tendency for turbulent interactions to maximize the entropy of the system.

Large Scale Air-Sea Interactions with a
Simple General Circulation Model

Abstract

We have coupled Lorenz's (1960) two-layer atomspheric model to
a "copper plate" ocean to obtain a simple model that can be used to
study the effects of large scale sea surface temperature anomalies on
the dynamics of the atmosphere. With 164 degrees of freedom, the
atmospheric model mimics the observed northern hemisphere energy cycle
in fair detail. In three experiments, each lasting one year, we con-
sider an ocean

(a) with fixed temperature that depends only on latitude;

(b) with fixed large amplitude SST anomalies; and

(c) with temperature determined by heat exchange with the air.

Only in (b) are significant dynamical effects observed. These consist
of a weak monsoon response in the subtropics and a tendency for storms
to intensify over warm water at higher latitude. Experiment (c) devel-
oped SST anomalies that resemble the observed anomalies; however, the
atmosphere and ocean in (c) differ insignificantly from the atmosphere
and recomputed "slave ocean" in (a), even when the flows are averaged
in reference frames moving with the anomalies. Our results suggest
that the atmosphere may be too noisy to be much affected by SST anoma-
lies on time scales over which the anomalies are themselves predictable.

1. Introduction

We wish to study the effects of large scale sea surface temperature anomalies, such as those described by Namias (1959), on the dynamics of the overlying atmosphere. By "anomaly" we mean the instantaneous departure of the sea surface temperature (SST) from its long-term time average. The persistence of SST anomaly patterns over time scales of months has led many people to believe that a better knowledge of these anomalies and their influence on the atmosphere could lead to improvements in long-term weather predictions. However, the associated heating anomalies are very small compared to many of the other fluxes that balance the heat budget of an atmospheric column; and it has therefore proved difficult to envision specific mechanisms by which SST anomalies might affect the weather. Our task is to weigh the relative importance of these two opposing features: long term persistence versus weakness of the signal.

The problem is complicated by the atmosphere's intrinsic lack of exact predictability. By this we mean that the equations governing atmospheric motion are ill-posed with respect to initial value problems in the sense that perturbations in the intital conditions at the smallest scales lead to completely different solutions after finite times. The cause of the growing difference is the propatation of the initial perturbation from the smallest to the largest scales of motion via the nonlinear terms in the Navier-Stokes equations. We can define an atmospheric predictability time scale, T_A, as the time required for a perturbation in the flow at the scale of the separation

between weather observing stations to reach the largest scales of motion. Theoretical and numerical estimates for T_A range between 5 days and about 3 weeks.

The existence of a limiting predictability time, T_A, for the atmosphere has important implications for the problem under study. First, it underscores the importance of studying forcing fields (such as SST) which have themselves a predictability time that is longer than T_A. The predictability time for sea surface temperature, T_O, is of the order of months because of the high heat capacity of the oceanic mixed layer and its relatively sluggish motion. Thus

$$T_O > T_A$$

and knowledge of the SST pattern ought to permit forecasts longer than T_A <u>provided</u> there is some <u>significant</u> connection between SST state and the state of the atmosphere above.

However, the limit on exact predictability suggests that this connection might at best be statistical. Consider the following hypothetical experiment: Imagine an ideal atmosphere whose external forcing fields (continents, oceans, solar heating, etc.) are freely controlled by us. Let $V(t)$ be any functional of the state of the atmosphere at time t. Let (1) denote some standard state for the forcing fields and let (2) denote some other forcing state (for example, a state with fixed SST anomalies). Now imagine two experiments beginning from the same initial conditions but subject to the

different forcing conditions (1) and (2). Let $V_1(t)$ and $V_2(t)$ be the outcomes of these experiments.

We should not be surprised if, after times longer than T_A, the two outcomes no longer resemble one another. However, it is misleading to attribute all of the difference $V_1 - V_2$ to the different forcing conditions (1) and (2). At any time, in fact, the major part of $V_1 - V_2$ is apt to be random, i.e. unpredictable; but we are interested only in that part of $V_1 - V_2$ that can be predicted. The predictable part of $V_1 - V_2$ will not be removed by statistical averaging. Therefore, we should compare not the outcomes themselves but rather their statistics.

It is plausible that the statistics of V depend only on the forcing (not on the initial conditions) and that the statistics change when the forcing changes. However, we should still want to know whether the statistical difference between V_1 and V_2 is large or small compared to the likely random differences.

For fixed forcing conditions, $V(t)$ is a stationary stochastic process with ensemble mean $\langle V \rangle$ which is independent of time. We find $\langle V \rangle$ by averaging $V(t)$ over many realizations, or, as is commonly done, by assuming $V(t)$ to be ergodic and averaging in time. The time-average estimator

$$\overline{V}_T = \frac{1}{T} \int_0^T V(t)dt$$

is a random variable with expected value $\langle V \rangle$ and standard deviation

proportional to $T^{-1/2}$ for large enough T. [1] That is, the average of V over a record of length T is "within" $const/T^{1/2}$ of $<V>$.

Now suppose $<V_1>$ and $<V_2>$ are the ensemble averages of V subject to the different fixed forcing conditons. Then the time, T_s, required for a change in forcing from state (1) to state (2) to make itself felt above the natural noisiness in V is given roughly by:

$$|<V_1> - <V_2>| = const_1/T_s^{1/2} + const_2/T_s^{1/2}$$

We might call T_s the "significance time scale" for V.

The pertinence of T_s to our problem is that if $T_s \gg T_o$ for any realizable change in SST state, then such changes are poor long term predictors of V because they are themselves destroyed by random processes before they can produce significant changes in V. If, on the other hand, $T_o > T_s$, then the field of SST may be a useful predictor of the quantity V. Said another way: if $T_o > T_s$, then the long persistence of SST anomalies overcomes the weakness of their heat fluxes; but if $T_s > T_o$, then the opposite is true.

By means of a mathematical model, we can, in principle,

---

[1] T is large enough if $\tau > T => |R(\tau)| \ll 1$ where

$$R(\tau) = \frac{<V(t)V(t + \tau)> - <V>^2}{<V^2> - <V>^2}$$

is the autocorrelation of V. See section 3 for a further discussion.

estimate the quantities $<V>$, const, and T_s and thereby determine

if and how knowledge of SST anomalies can help to extend forecasts.

In the following pages we present the results of such a study. By

way of overall summary, we find that, for several quantities of

interest studied in our simple model, T_s is of the order of T_o or

longer, so that knowledge about SST anomalies would not greatly extend

forecasts. However, our conclusions depend on the many simplfying

assumptions we have made and may well be altered by future work.

2. The Model

We are interested in the behavior of the coupled ocean/ atmosphere system over time scales of months -- the time scales in which SST anomalies are observed to appear and disappear. Such times are long compared to T_A and to the energy transit time through the atmospheric spectrum. Consequently, we require a somewhat sophisticated model for the atmosphere -- one that correctly simulates the many nonlinear processes that maintain the global general circulation against dissipation. In order to accommodate nonlinear transfers of energy over a range of scales, the atmospheric model must be a numerical one. As such, it must be both economical and computationally stable with respect to the relatively long time integrations required for statistical averaging. To satisfy these requirements, we have adopted a simple atmospheric model invented by Lorenz (1960).

Our ocean model can likely be far simpler, because a time scale of months is possibly still short compared to the time required for ocean currents to greatly alter an SST anomaly pattern whose features are several thousand kilometers in diameter. To begin with, we will ignore ocean motion altogether; our model ocean will be a stationary heat reservoir covering the globe.

In the two-layer version of Lorenz's atmospheric model the dependent variables are:

$\psi + \tau$ the streamfunction at 250 mb

$\psi - \tau$ the streamfunction at 750 mb

$\theta + \sigma$ the potential temperature at 250 mb

7

$\theta - \sigma$ the potential temperature at 750 mb

$$X \equiv -\frac{1}{\Delta p} \int_{0}^{\Delta p} \xi(p)\,dp$$

the vertical average of the velocity potential

($\Delta p = 500$ mb).

In terms of the above variables, the two-layer equations take the form:

$$\nabla^2 \psi_t + J(\psi, \nabla^2\psi + f) + J(\tau, \nabla^2\tau) = F_\psi \tag{1.1}$$

$$\nabla^2 \tau_t + J(\tau, \nabla^2\psi + f) + J(\psi, \nabla^2\tau) - \nabla\cdot(f\nabla X) = F_\tau \tag{1.2}$$

$$\theta_t + J(\psi, \theta) + J(\tau, \sigma) - \nabla\cdot(\sigma\nabla X) = H_\theta \tag{1.3}$$

$$\sigma_t + J(\psi, \sigma) + J(\tau, \theta) - \nabla\theta\cdot\nabla X = H_\sigma \tag{1.4}$$

$$bC_p \nabla^2\theta = \nabla\cdot(f\nabla\tau) \tag{1.5}$$

where

$$b = \frac{1}{2}\left\{ \left(\frac{3}{4}\right)^\kappa - \left(\frac{1}{4}\right)^\kappa \right\} = .124$$

and $\kappa \equiv R/C_p \equiv$ (gas constant)/(heat capacity at constant pressure).

Here, F_ψ, F_τ, H_θ, H_σ are the friction and heating terms. The above equations are very nearly the conventional quasi-geostrophic approximation, except that the variability of Coriolis parameter, f, is retained in all terms. The method of vertical differencing incorporates the boundary conditions $\omega \equiv \frac{dp}{dt} = 0$ at $p = 1000$ mb and $p = 0$. The vertical velocity at 500 mb is assumed to be $\omega_{500} = \Delta p \, \nabla^2 \chi$.

Lorenz showed that, under adiabatic conditions, the equations (1.1 - 1.5) conserve the sum of

$$K = \frac{\Delta p}{g} \left[\nabla \psi \cdot \nabla \psi + \nabla \tau \cdot \nabla \tau \right] \tag{1.6}$$

and

$$A = \frac{2 b C_p \, \Delta p}{g} \frac{\left[(\theta')^2 + (\sigma')^2 \right]}{[\sigma] + [\sigma^2 + (\theta')^2]} \tag{1.7}$$

which are the vertical-finite-difference analogs of the kinetic and available potential energy per unit area. Here, the brackets ([ ]) denote the area average over a region on whose boundary the normal velocity vanishes; and

$$\theta' \equiv \theta - [\theta] \quad , \quad \sigma' \equiv \sigma - [\sigma]$$

The requirement that the vertically-differenced equations (1.1 - 1.5) conserve quantities that are analogous to the adiabatic invariants of the exact equations accomplishes two things:

1) It virtually assures computational stability of the differenced equations.

2) It permits us to analyze the energy budget of solutions to the differenced equations.

For a detailed development of the differenced equations and energy invariants the reader is referred to Lorenz's original paper.

We complete the set of model equations with a thermal equation for the ocean:

$$\frac{\partial \theta_w}{\partial t} = H_w \qquad (1.8)$$

We solve the equations (1.1 - 1.5, 1.8) spectrally by expanding the dependent variables in terms of spherical harmonic functions:

$$(\psi, \tau, \theta, \sigma, \chi, \theta_w) = \sum_{n=0}^{\infty} \sum_{m=-n}^{+n} (\psi_n^m, \theta_n^m, \tau_n^m, \sigma_n^m, \chi_n^m, \theta_{w_n}^m) Y_n^m(\alpha, \varphi)$$

and then truncating the series to include only certain pre-chosen harmonics. Here,

$$Y_n^m(\alpha, \varphi) = \left\{ \frac{2n+1}{4\pi} \frac{(n-|m|)!}{(n+|m|)!} \right\}^{1/2} P_n^{|m|}(\cos \alpha) \, e^{im\varphi}$$

where α is the colatitude, φ the longitude, and P_n^m an associated Legendre's function. Y_n^m has m oscillations running east-west around the globe and $n - |m|$ zero-crossings between the north and south poles. As is well known, the spherical harmonics comprise a complete set of orthogonal functions and satisfy the eigenvalue relation

$$\nabla^2 Y_n^m = - \frac{n(n+1)}{r_e^2} Y_n^m$$

where r_e is the earth's radius.

The somplete set of coupled ordinary differential equations are as follows:

$$K(K+1)\frac{d\Psi_K^j}{dt} = -\frac{1}{r_e^2}\sum_{\langle n,m\rangle}\sum_{\langle r,s\rangle}\left(\Psi_n^m\Psi_r^s+\tau_n^m\tau_r^s\right)r(r+1)\times$$

$$\times E_{nrk}^{ms-j} + 2\Omega\sqrt{-1}\,j\Psi_K^j - r_e^2(F_\Psi)_K^j \tag{1.9}$$

$$K(K+1)\frac{d\tilde{\tau}_K^j}{dt} = -\frac{1}{r_e^2}\sum_{\langle n,m\rangle}\sum_{\langle r,s\rangle}\left(\tau_n^m\Psi_r^s+\Psi_n^m\tilde{\tau}_r^s\right)r(r+1)\times \tag{1.10}$$

$$\times E_{nrk}^{ms-j} - \Omega\left(4\pi/3\right)^{1/2}\sum_{(r,s=j)}\chi_r^j\left\{2-r(r+1)-k(k+1)\right\}A_{Irk}^{oj-j}+$$

$$+ 2\Omega\sqrt{-1}\,j\tilde{\tau}_K^j - r_e^2(F_{\tilde{\tau}})_K^j \tag{1.11}$$

$$\frac{d\Theta_K^j}{dt} = -\frac{1}{r_e^2}\sum_{\langle n,m\rangle}\sum_{(r,s)}\left(\Psi_n^m\Theta_r^s+\tau_n^m\sigma_r^s\right)E_{nrk}^{ms-j}+$$

$$+ \sum_{(n,m)}\sum_{(r,s)}\frac{\sigma_n^m\chi_r^s}{2r_e^2}\left\{n(n+1)-r(r+1)-k(k+1)\right\}A_{nrk}^{ms-j}+(H_\Theta)_K^j \tag{1.12}$$

$$\frac{d\sigma_K^j}{dt} = -\frac{1}{r_e^2}\sum_{\langle n,m\rangle}\sum_{(r,s)}\left(\Psi_n^m\sigma_r^s+\tau_n^m\Theta_r^s\right)E_{nrk}^{ms-j}+$$

$$+ \sum_{(n,m)}\sum_{(r,s)}\frac{\Theta_n^m\chi_r^s}{2r_e^2}\left\{n(n+1)+r(r+1)-k(k+1)\right\}A_{nrk}^{ms-j}+(H_\sigma)_K^j \tag{1.13}$$

$$-bC_p K(k+1)\Theta_K^j = \sum_{\langle r,s=j\rangle}\tau_r^j\,\Omega\left(4\pi/3\right)^{1/2}\left\{2-r(r+1)-k(k+1)\right\}A_{Irk}^{oj-j}$$

$$\frac{d\Theta_w{}^j{}_k = (H_w)^j{}_k \tag{1.14}$$

In the above equations the symbol $\underset{\langle n,m \rangle}{\Sigma}$ refers to that part of $\overset{\infty}{\underset{n=0}{\Sigma}} \overset{+n}{\underset{m=-n}{\Sigma}}$ that includes only the finite set of "velocity harmonics" -- the harmonics chosen to represent ψ and τ. Similarly, $\underset{(n,m)}{\Sigma}$ refers to that part of $\overset{\infty}{\underset{n=0}{\Sigma}} \overset{+n}{\underset{m=-n}{\Sigma}}$ that includes only the "thermal harmonics" representing θ, σ, χ, and θ_w. To reduce the possible number of degrees of freedom, we assume that the flow is symmetric about the equator. In this case, the velocity harmonics include only functions $Y_n{}^m$ for which $n - |m|$ is odd; whereas the thermal harmonics have $n - |m|$ even. The expressions A_{nrk}^{msj} and E_{nrk}^{msj} are the Adams and Elsasser integrals defined by

$$A_{nrk}^{msj} = \int_0^{\pi} \sin\alpha \, d\alpha \int_0^{2\pi} d\varphi \, Y_n{}^m Y_r{}^s Y_k{}^j$$

and

$$E_{nrk}^{msj} = \int_0^{\pi} d\alpha \int_0^{2\pi} d\varphi \left\{ \frac{\partial Y_n{}^m}{\partial \alpha} \frac{\partial Y_r{}^s}{\partial \varphi} - \frac{\partial Y_n{}^m}{\partial \varphi} \frac{\partial Y_r{}^s}{\partial \alpha} \right\} Y_k{}^j.$$

James (1973) gives a formula for evaluating these integrals. In equation (1.13), it can be shown that $A_{1rk}^{oj-j} = 0$ unless $r = k \pm 1$. Thus $\theta_n{}^m$ is coupled to $\tau_{n+1}{}^m$ and $\tau_{n-1}{}^m$ via the thermal wind relation.

Under adiabatic conditions, the spectrally-truncated differenced equations conserve the sum of the spectral truncations of

(1.6) and (1.7). We shall refer to

$$K_n^m = \frac{\Delta P}{4\pi g \, r_e^2} \left\{ |\psi_n^m|^2 + |\tilde{\tau}_n^m|^2 \right\} n(n+1)(2-\delta_{om}), \quad m \geqslant 0$$

and

$$A_n^m = \frac{2 b C_p \, \Delta P}{g \, (4\tilde{\pi})^{1/2}} \, \frac{\left\{ |\theta_n^m|^2 + |\sigma_n^m|^2 \right\} (2-\delta_{om})}{\theta_o^o + \left\{ \sum\limits_{(r,s)} \left(|\theta_r^s|^2 + |\sigma_r^s|^2 \right) - \theta_o^{o2} \right\}^{1/2}}, \quad n \neq 0, \; m \geqslant 0$$

as the kinetic and available potential energy in mode n-m.

We solve the prognostic equations (1.9 - 1.12, 1.14) with a predictor/corrector time-stepping scheme. Although there is no prognostic equation for χ, we can obtain a set of diagnostic equations for χ_n^m in terms of the prognostic variables ψ, $\tilde{\tau}$, θ, σ, θ_w by replacing (1.13) with its time derivative and substituting from equations (1.10) and (1.11) for $\frac{d\tilde{\tau}^j}{dt}$ and $\frac{d\theta_k^j}{dt}$. The resulting equations can be simplified in their general form and solved by Gaussian elimination on the computer.

It remains to specify the friction and heating terms. They are:

$$\overset{(a)}{} \qquad \overset{(e)}{}$$
$$F_\psi = - \frac{k^*}{2} \nabla^2 \psi_s - E_\psi \tag{1.15}$$

$$\overset{(a)}{} \qquad \overset{(b)}{} \qquad \overset{(e)}{}$$
$$F_{\tilde{\tau}} = + \frac{k^*}{2} \nabla^2 \psi_s - 2\ell \nabla^2 \tilde{\tau} - E_{\tilde{\tau}} \tag{1.16}$$

$$(c) \qquad (d) \qquad (e)$$
$$H_\theta = -k_T(\theta - \theta^*) + \frac{\lambda_1}{2}(\theta_w - \theta_s) - E_\theta \qquad (1.17)$$

$$(c) \qquad (d) \qquad (e)$$
$$H_\sigma = -h(\sigma - \sigma^*) - \frac{\lambda_1}{2}(\theta_w - \theta_s) - E_\sigma \qquad (1.18)$$

$$(d)$$
$$H_w = -\lambda_2(\theta_w - \theta_s) \qquad (1.19)$$

where ψ_s and θ_s are the surface streamfunction and air temperature (Eq. 1.23). The terms designated by letters represent the effects of:

(a) friction with the ground, and

(b) between levels;

(c) net radiational convergence, mean sensible and latent heat transfer, and small scale vertical mixing in driving the atmosphere toward a steady state: $\theta = \theta^*$, $\sigma = \sigma^*$ that would prevail in the absence of large scale flow;

(d) anomalous latent and sensible heat exchange between the ocean and lower troposphere; and

(e) small scale horizontal mixing.

The terms (a) can, if one desires, be thought of as an Ekman friction in which case

$$W_{Ekman} = \frac{\Delta p \, k^*}{P_s \, g}\left(\frac{\nabla^2 \psi_s}{f}\right) \qquad (1.20)$$

In (d) the anomalous heat flux from ocean to atmosphere is assumed to obey:

$$\text{flux} = \lambda (\theta_w - \theta_s) \tag{1.21}$$

so that

$$\lambda_1 = \left(\frac{4}{3}\right)^x \frac{g \lambda}{\Delta p \, C_P} \qquad \text{and} \qquad \lambda_2 = \frac{\lambda}{\rho_w \, C_{Pw} \, D} \tag{1.22}$$

where D is the depth of the oceanic mixed layer (assumed constant) and subscript "w" refers to ocean variables. We express the surface variables in terms of the model variables by:

$$\psi_s = \psi - \gamma \tau \quad , \qquad \theta_s = \theta - \gamma \sigma \tag{1.23}$$

If ψ and θ are linear in pressure then $\gamma = 2$. However, it is more realistic to assume that the variables are linear in height, in which case $\gamma = 1.6$ for a "standard atmosphere".

The above extremely crude parameterization abstracts the atmospheric heating field into two parts: a part that is correlated with the temperature of the lower bounding surface and a part that is independent of it. Both parts are characterized by equilibrium states $(\theta^*, \sigma^*; \theta_w)$ and return time scales $(\frac{1}{K_T}, \frac{1}{h}; \frac{2}{\lambda_1})$. We have tentatively assumed that these time scales are equal:

$$\frac{1}{K_T} = \frac{1}{h} = \frac{2}{\lambda_1}$$

and adjusted their values, along with the other parameters in (1.15 - 1.19), to obtain a model general circulation whose spectral energetics agree reasonably well with Saltzman's (1970) summary of the observational data. The values we arrived at are the following:

$$\frac{1}{k^*} = 2.55 \text{ days} \qquad \frac{1}{\ell} = 67.9 \text{ days}$$

$$\frac{1}{k_T} = \frac{2}{\lambda_1} = \frac{1}{h} = 10.2 \text{ days}$$

$$\frac{1}{\lambda_2} = 41.6 \text{ days and } \infty \text{ days}$$

$$\sigma^* = 12.5 \text{ C}$$

and

$$\begin{Bmatrix} E_\psi \\ E_\tau \\ E_\theta \\ E_\sigma \end{Bmatrix} = \begin{Bmatrix} \sum_{\langle n,m \rangle} -\frac{n^2(n+1)^2}{r_e^2} \\ \sum_{\langle n,m \rangle} n(n+1) \end{Bmatrix} (.00016 \text{ day}^{-1}) \begin{Bmatrix} \psi_n^m \\ \tau_n^m \\ \theta_n^m \\ \sigma_n^m \end{Bmatrix} Y_n^m$$

The value of k^* corresponds to $\frac{\Delta p \, k^*}{P_s \, g} = 3.12 \text{ cm-sec}^{-1}$ in (1.20). Our choice of λ_1 corresponds to $\lambda = 22.3 \text{ ly-day}^{-1}\text{-deg}^{-1}$ which is smaller than the value of 63.1 used by Doos (1962). The two extreme values of λ_2 correspond to D = 9.3 meters and D = ∞ (constant temperature ocean). The eddy viscosity is quite modest; at the

highest wavenumbers considered it amounts to only about one fourth the ground friction. θ^*, which is assumed proportional to Y_2^0 is sketched in Figure 1.4.

We do not permit the model to determine its own globally-averaged temperature but set $\theta_0^0 = \theta_{W_0}^0 = 0$ throughout. Thus the only globally-averaged temperature of physical significance is σ_0^0, which is proportional to the average temperature difference between 250 mb and 750 mb. For σ_0^0 only, we use

$$\left(H\sigma \right)_0^0 = -\left(k + \frac{\lambda_1}{2} \right) \left(\sigma_0^0 - \sigma_0^{0^*} \right) \tag{1.24}$$

instead of (1.18). σ^* is chosen so that the equilibrium σ is less than its value in Nature. In this way, we model implicitly the destabilizing influence of water vapor in the earth's atmosphere.

The computer program that solves the model equations is written in a general form that accepts any basic set of spherical harmonic functions. The choice of specific set is to some extent arbitrary, but the chosen harmonics should accommodate spectral energy transfers analogous to those which are known to be important in the real atmosphere. Table 1.1 presents the set of harmonics we have used in the experiments in section 3. It consists of a zonal flow and 4 zonal wavenumbers, each with 3 degrees of freedom in the north-south direction. The chosen zonal harmonics are just sufficient to resolve the classical three-cell (Hadley, Ferrel, polar) structure of the general circulation.

Our restrictive choice of harmonics drastically under-represents the influence of the higher wavenumbers in the flow, whose principal dynamical effect is assumed to be the destruction of accuracy in deterministic forecasts on a time scale of T_A.[2] We assume a *priori* that for times longer than T_A, only the statistics of the large scale flow are pertinent; and we direct our research to the questions:

1) How do the stationary statistics of our atmosphere change when the properties of the ocean model are changed?

2) How long must one average to detect these statistical changes above the random noise in the large scale flow?

Our approach is strictly valid only if unresolved small scales exert no ocean-sensitive effects on the large scale statistics, and if the random noise in large scales can be reasonably well mimicked by a model that includes only large scales.

While a rigorous justification of our method awaits careful experimentation with higher resolution models, we are encouraged by the resemblance of some statistics of our simple model with those based on real observations. Figure 1.1 compares the model energy cycle, averaged over 357 days, with Saltzman's (1970) observed energy cycle (band averaged in zonal wavenumber m) for winter and summer. The overall agreement between model and atmosphere is good except for the

---

[2] The time required for the propagation of order one error from the smallest scales resolved in our model to the largest scales is less than three days.

TABLE 1.1

The set of harmonics used in the experiments described in this paper.

Harmonic n-m refers to Y_n^m.

Velocity Harmonics

5-0	8-3	11-6	14-9	17-12
3-0	6-3	9-6	12-9	15-12
1-0	4-3	7-6	10-9	13-12

Thermal Harmonics

6-0				
4-0	7-3	10-6	13-9	16-12
2-0	5-3	8-6	11-9	14-12
0-0	3-3	6-6	9-9	12-12

model wavenumber 3. Further experiments have shown that the situation improves considerably when we include mountain ranges and large scale stationary heating, which are known to force the very long waves. Figure 1.2 compares the model average flow fields with the observations. Generally speaking, our simulation resembles the atmosphere under winter conditions except for the imposed equatorial symmetry.

The method of spectral solution has been applied extensively to Lorenz's model (minus the ocean) by other investigators. However, ours is the first application (of which we are aware) that allows the static stability σ to vary in space. The static stability is known from both theory and experiment to exert an important control on flow in rotating, differentially-heated fluids. Moreover, static stability and SST may be correlated in Nature; Namias (1973) has shown that when SST anomalies are large, there is sometimes good correlation between SST anomaly and the thickness (temperature) of the air below 750 mb.

Solving equations (1.9-1.14) with the harmonics in Table 1.1 amounts to time-stepping 164 coupled nonlinear real ordinary differential equations. With a time step of .25 days, one year's climatic simulation requires about 3.25 minutes of CPU time on a 7600 computer at a cost of about $32.

Figure 1.1

Comparison of the model energy cycle averaged over one year with Saltzman's (1970) observations (band averaged in zonal wavenumber m) for winter (in brackets) and for summer (in parentheses). Boxes represent energy in 10^5 joules m^{-2}. Arrows represent fluxes in watts m^{-2}. Both the definition of energy quantities and the spectral truncation differ between our model and the Saltzman data, so that the comparison is not intended to be exact. The conversion arrows give the gain of kinetic energy in each band from the total available potential energy. The spurious energy loss from the highest wavenumbers in the model would disappear if the time step were reduced.

AVAILABLE
POTENTIAL ENERGY

KINETIC ENERGY

GENERATION

DISSIPATION

2.89
[3.00]
(1.70)

Observed: m = 0
Model:
2-0, 4-0, 6-0
45.5
[35.5] (22.8)

.30
[0]

Observed: m = 0
Model:
1-0, 3-0, 5-0
12.1
[10.0] (5.6)

.60
[.48]

2.40
[5.25]
(1.65)

.30
[.48]
(.65)

.27
[.96]
(.08)

m = 1, 2, 3, 4
Model:
3-3, 5-3, 7-3
.6
[8.0] (4.6)

.01
[.21]
(.30)

m = 1, 2, 3, 4
Model:
4-3, 6-3, 8-3
.9
[7.9] (4.3)

.20
[1.10]

.41
[2.44]
(.33)

.15
[1.02]

.04
[.29]
(.10)

.46
[.52]
(.19)

m = 5, 6, 7
Model:
6-6, 8-6, 10-6
1.1
.[1.9] (1.4)

.14
[.18]
(.16)

m = 5, 6, 7
Model:
7-6, 9-6, 11-6
3.0
[3.3] (2.8)

.36
[.73]

1.00
[1.05]
(.78)

.61
[1.18]

.11
[.30]
.(.15)

.24
[.12]
(.09)

m = 8, 9, 10
Model:
9-9,11-9,13-9
.5
[.9] (.6)

.12
[.09]
(.12)

m = 8, 9, 10
Model:
10-9,12-9,14-9
3.0
[2.1] (1.8)

.35
[.11]

.80
[.84]
(.44)

.62
[.66]

.08
[.11]
(.10)

.18
[.25]
(.10)

m = 11, 12, 13
Model:
12-12,14-12,16-12
.2
[.3] (.3)

.03
[.03]
(.05)

m = 11, 12, 13
Model:
13-12,15-12,17-12
.9
[.7] (.7)

.14
[.04]
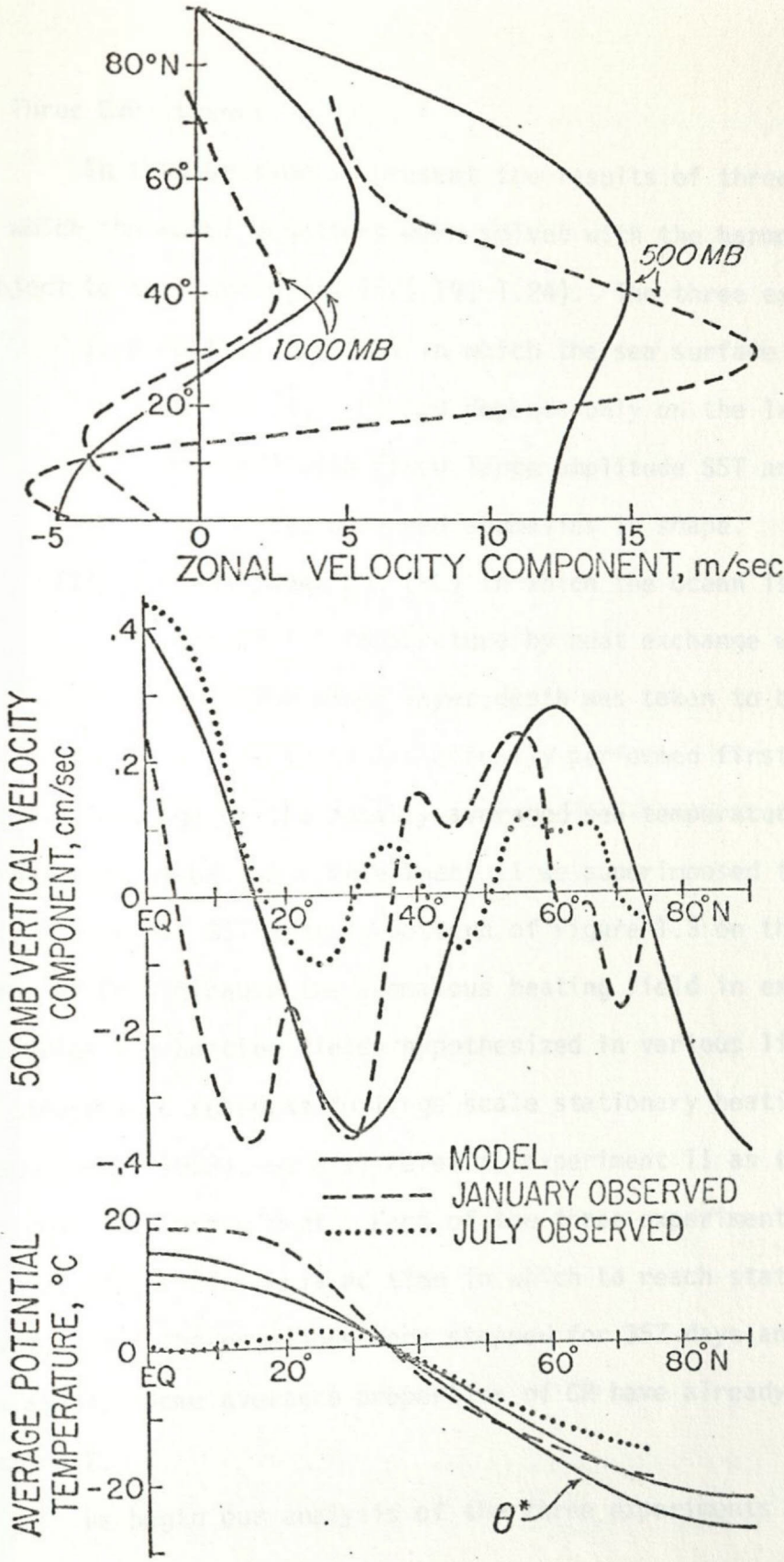(.06)

.10
[.01]
(.00)

.08
[.14]

.10
[.06]

Figure 1.2 Average flow quantities in the model and in the real atmosphere. The average temperature presented is the actual temperature minus the temperature at 35 N. Observations are from Oort and Rasmusson, Tables A8, A9 and F8.

3. Three Experiments

In this section we present the results of three experiments in which the model equations were solved with the harmonics in Table 1.1 subject to the forcing (1.15-1.19, 1.24). The three experiments are:

I. A control run (CR) in which the sea surface temperature is fixed ($\lambda_2 = 0$) and depends only on the latitude.

II. A run (WM) with fixed large amplitude SST anomalies that resemble the observed anomalies in shape.

III. A mixed layer run (ML) in which the ocean is free ($\lambda_2 \neq 0$) to adjust its temperature by heat exchange with the atmosphere. The mixed layer depth was taken to be 10 meters.

The mixed layer experiment was actually performed first. We then used the time average of the zonally averaged sea temperature in ML for the fixed ocean in CR. For experiment II we superimposed the longitudinally-sinusoidal SST anomaly pattern of Figure 1.3 on the standard ocean of CR. Because the anomalous heating field in experiment II resembles the heating fields hypothesized in various linear theories of atmospheric response to large scale stationary heating (for example, Smagorinsky, 1953), we will refer to experiment II as the "weak monsoon" (WM) experiment. Each of the three experiments was allowed several months of simulated time in which to reach statistical equilibrium. Then the equations were stepped for 357 days and all the data was saved. Some averaged properties of CR have already been given in section 2.

We begin our analysis of the three experiments by showing that

the different ocean models cause no statistically significant difference in the globally-averaged energy cycle. First, however, we describe the very simple format we have used to compare statistical averages: Let $V(t)$ be any quantity and suppose we wish to compare the average of V in run 1 with its average in run 2. We divide each run of length T into N subintervals of equal length T/N and form the average of V over each subinterval. Let $\overset{i}{V}$ be the average over the i-th subinterval. Then the average of V over the entire record in run j is:

$$\overline{V_j} = \frac{1}{N} \sum_{i=1}^{N} \overset{i}{V_j}$$

We assume that the subintervals are sufficiently long so that $\overset{i}{V}$ and $\overset{k}{V}$ are independent random variables if $i \neq k$. Then the variance of $\overset{i}{V}$, assumed independent of i, is given by the (unbiased) estimator:

$$\sigma^2 = \frac{1}{N-1} \sum_{i=1}^{N} (\overset{i}{V} - \overline{V})^2$$

and the standard deviation of $\overline{V}$ is:

$$\hat{\sigma} = \sigma / N^{1/2}$$

We define a "significance parameter" for the difference between $\overline{V}_1$ and $\overline{V}_2$ by:

$$S_{1,2} = |\overline{V_1} - \overline{V_2}| / (\hat{\sigma_1} + \hat{\sigma_2})$$

When $S_{1,2}$ is larger than unity then $\overline{V}_1$ and $\overline{V}_2$ differ by a statistically significant amount. [3] For large $S_{1,2}$ we have the

---

[3] For example, if V_1 and V_2 are Gaussian with $<V_1> = <V_2>$, then the probability that $S_{1,2}$ exceeds unity is 31.7%. Most of the quantities analyzed appear not to be Gaussian, however.

following (biased) estimate of the quantity T_s defined in section 1:

$$T_s \sim \frac{1}{S_{1,2}^2} T \qquad (1.26)$$

For $S_{1,2} < 1$ we can say only that $T_s > T$. If $V(t)$ contains significant energy at periods longer than T/N then the above method underestimates the significance of the difference between $\overline{V}_1$ and $\overline{V}_2$. Since all of the model variables analyzed in the above manner had computed spectra that were white or blue at periods exceeding one month, we have chosen $T = 357$ days and $N = 10$.

Table 1.2 summarizes the global energy cycles of the three experiments. The quantities tabulated are the same as those diagrammed in Figure 1.1 for CR only. From the last two colums of Table 1.2 we see that if statistical differences exist between the three energy cycles, they apparently cannot be detected above the random noise in time averages of one year or less.

Of course, it is not especially surprising that space-time averages should be similar in the three experiments, because all three have the same time-longitude averaged sea temperature. It is more likely that the experiments have different average spatial distributions of certain quantities and that the distributions are correlated in some way with the SST anomaly pattern. Figure 1.3 shows the average surface streamfunction in WM. A stationary signal is present in the form of a low level ridge centered near the meridian of maximum cooling. At upper levels, the ridge becomes a trough that is barely

Table 1.2   Energy Cycles of the Three Experiments

Quantity	m	357-day average			estimated			significance parameter	
		I-CR	II-WM	III-ML	I	II	III	$S_{I,II}$	$S_{I,III}$
Kinetic energy	0	12.06	11.90	12.32	.10	.12	.24	.76	.77
in zonal	3	.94	1.00	.87	.09	.07	.11	.43	.33
wavenumber m	6	3.02	2.80	2.82	.20	.14	.36	.63	.35
	9	2.95	3.00	2.80	.31	.23	.26	.10	.26
$(10^5$ joule m$^{-2})$	12	.92	.87	.82	.07	.06	.04	.40	.95
Available pot.	0	45.46	45.57	45.73	.38	.55	.75	.11	.23
energy in m	3	.64	.74	.62	.04	.04	.06	1.19	.12
$(10^5$ joule m$^{-2})$	6	1.07	1.02	1.15	.08	.07	.12	.35	.38
	9	.51	.54	.50	.05	.05	.05	.28	.19
	12	.17	.16	.17	.01	.01	.01	.75	.02
Conversion of	0	.30	.29	.33	.02	.01	.02	.43	.63
APE to KE	3	.15	.19	.15	.02	.02	.02	1.00	.07
in m	6	.61	.54	.56	.06	.04	.05	.70	.51
(watt m$^{-2})$	9	.62	.68	.60	.07	.07	.06	.38	.16
	12	.08	.07	.08	.02	.02	.02	.29	.12
Generation of	0	2.89	2.87	2.85	.05	.08	.10	.14	.21
APE in m	3	-.27	-.27	-.26	.02	.02	.03	.07	.21
(watt m$^{-2})$	6	-.46	-.44	-.50	.04	.03	.06	.35	.38
	9	-.24	-.25	-.23	.02	.02	.02	.27	.21
	12	-.10	-.09	-.09	.01	.005	.01	.74	.45
Transfer of	0	-2.39	-2.39	-2.34	.05	.07	.08	.04	.35
APE to m	3	.41	.45	.39	.03	.04	.04	.64	.20
by	6	1.00	.92	1.00	.08	.07	.09	.54	.03
temperature	9	.80	.86	.77	.08	.08	.08	.38	.18
advection	12	.18	.16	.18	.03	.02	.02	.12	.01
(watt m$^{-2})$									
Nonlinear	3	.01	.02	.01	.01	.01	.004	.75	.08
transfer of	6	.14	.13	.10	.01	.01	.01	.54	1.27
KE to zonal	9	.12	.12	.12	.01	.01	.02	.04	.05
flow by m	12	.03	.03	.02	.003	.003	.004	.33	1.53
(watt m$^{-2})$									
Gain of KE by	3	.04	.03	.04	.02	.02	.01	.28	.10
m due to wave	6	-.11	-.08	-.07	.03	.02	.02	.48	.68
interactions	9	-.08	-.10	-.08	.03	.03	.02	.28	.01
(watt m$^{-2})$	12	.14	.14	.11	.01	.02	.01	.03	1.20
Gross static		166.01	165.98	165.78	.19	.17	.23	.10	.55
stability									
$(10^5$ joule m$^{-2})$									

detectable in the strong westerly flow. The signal in Figure 1.3 is
statistically significant ($S_{...}$ exceeds 3.0) and agrees approxi-
mately with linear theory. It is interesting, however, that the
maximum response occurs in the subtropics (25 N lat.) and not at the
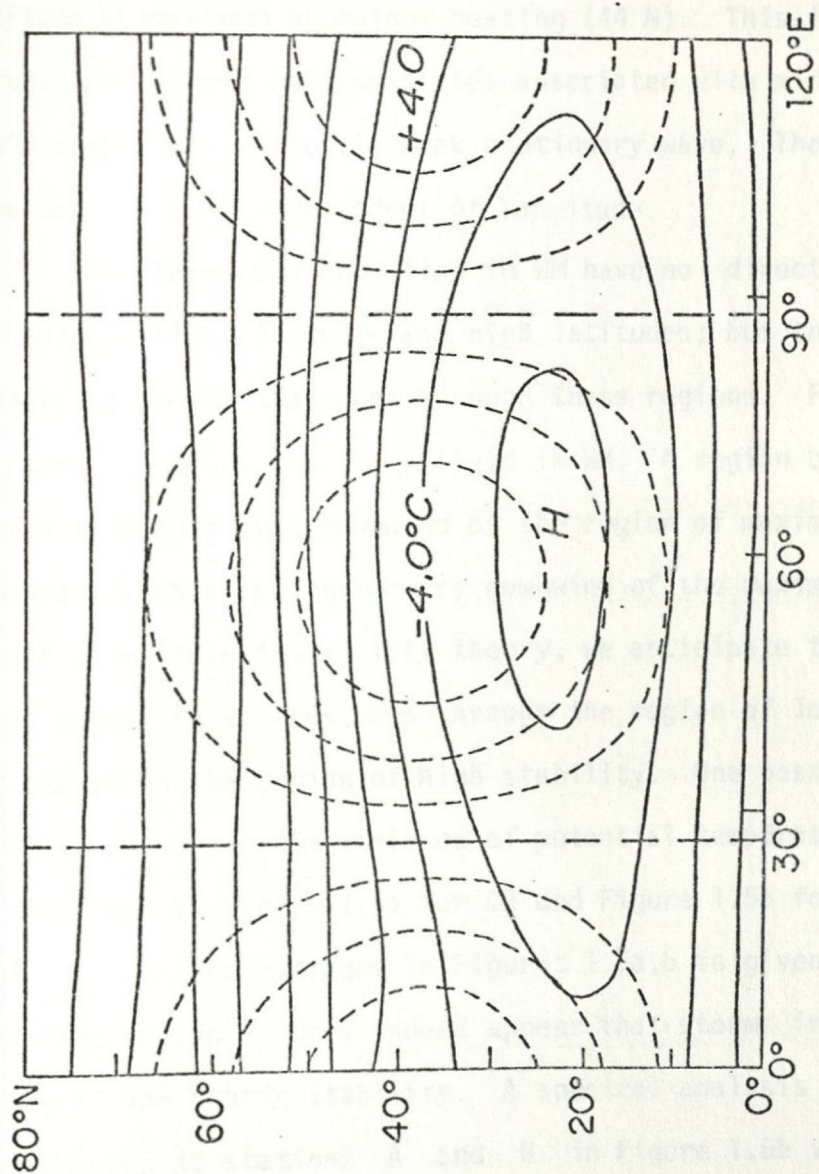latitude of maximum diabatic heating (44 N). This anomaly

Figure 1.3 SST anomaly pattern and average surface streamfunction in WM. The SST anomaly extrema are ± 4.0 C. The maximum wind speed is 6 m-sec^{-1}. The maximum streamfunction (difference from the control run) of 1 mb occurs at 25 N.

detectable in the strong westerly flow. The signal in Figure 1.3 is statistically significant ($S_{I, II}$ exceeds 3.0) and agrees approximately with linear theory. It is interesting, however, that the maximum response occurs in the subtropics (25 N lat.) and not at the latitude of maximum anomalous heating (44 N). This is apparently because the strong nonlinearities associated with mid-latitude storms would completely disrupt a weak stationary wave. The average stream-function in CR is independent of longitude.

The large SST anomalies in WM have no direct influence on the average flow at middle and high latitudes; but they may affect the travelling storms that pass through these regions. Figure 1.4 shows the average static stability field in WM. A region of low static stability occurs just downwind of the region of maximum surface heating and a stable regions occurs downwind of the maximum cooling. From linear baroclinic instability theory, we anticipate that the storms might intensify as they pass through the region of low static stability and weaken in the region of high stability. One possible index of storm intensity is the variance of potential temperature which is mapped at sea level in Figure 1.5a for CR and Figure 1.5b for WM. The field of $S_{I, II}$ for the averages in Figures 1.5a,b is given in Figure 1.5c. From Figure 1.5b it does indeed appear that storms intensify in the region of low static stability. A spectral analysis of the temperature records at stations A and B in Figure 1.5b verifies that the larger variance of θ_s at station A is primarily caused by the intensification of disturbances with periods between 3 and 9 days.
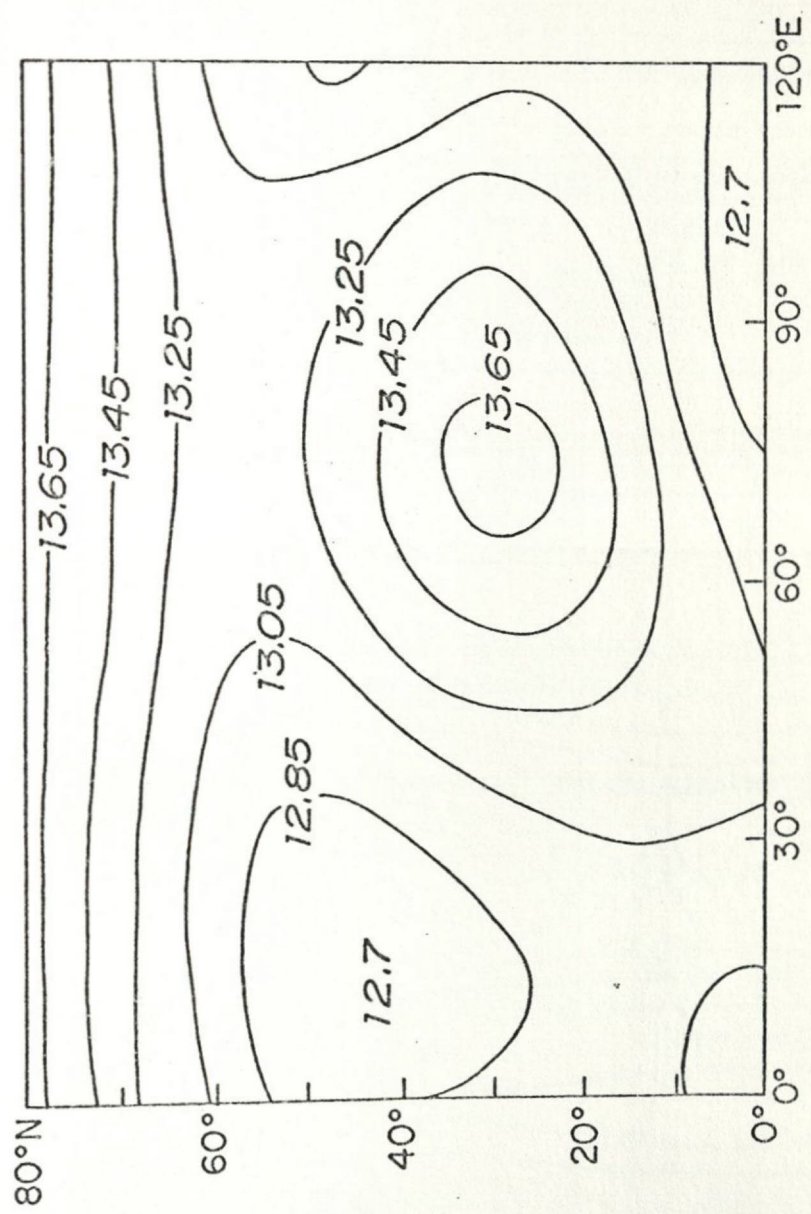
Figure 1.4 Average static stability, σ, in experiment WM (degrees centigrade).

Figure 1.5a

The variance of sea level potential temperature

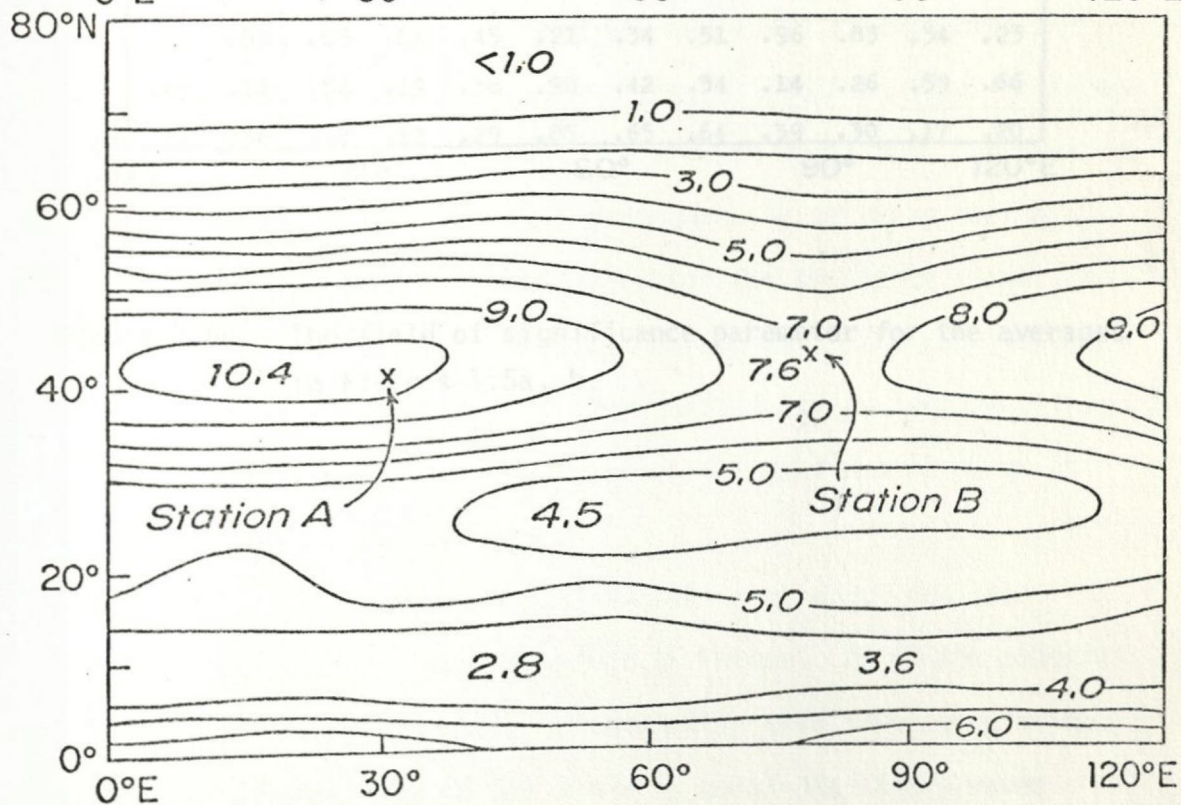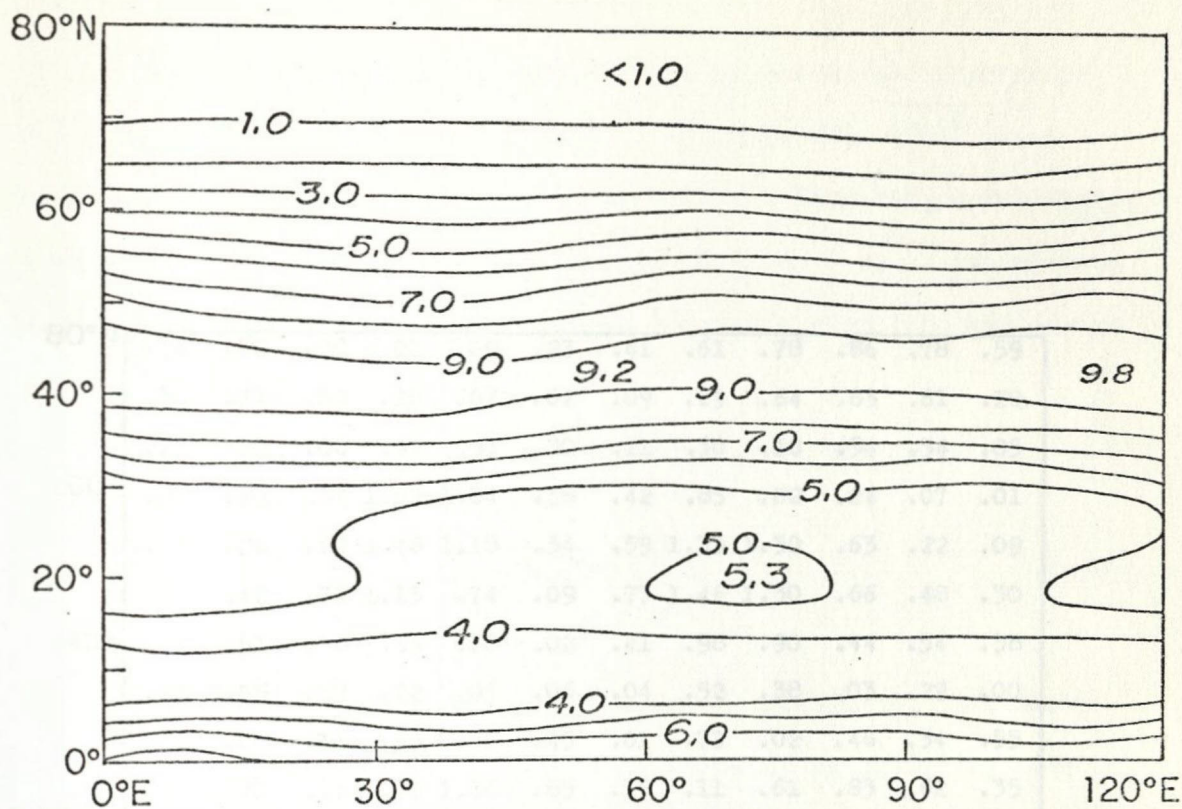$$\overline{(\theta'_s)^2} = \overline{\theta_s^2} - \overline{\theta_s}^2$$

in deg^2 in CR.

Figure 1.5b

The variance of sea level potential temperature

$$\overline{(\theta'_s)^2} = \overline{\theta_s^2} - \overline{\theta_s}^2$$

in deg^2 in WM.

Figure 1.5c   The field of significance parameter for the averages
in Figures 1.5a, b.

Figures 1.6 a, b show the variance of potential temperature at 500 mb in the same two experiments. Again in WM, $\overline{(\theta')^2}$ is a maximum in the region of low static stability. Somewhat surprisingly, however, $\overline{(\theta')^2}$ also shows a maximum in CR (Fig. 1.6a). The maximum in CR is not correlated with a minimum in static stability and occurs purely by chance.

Still another index of storm intensity is the quantity

$$\overline{w'\theta'} = \overline{w\theta} - \overline{w}\,\overline{\theta} \tag{1.27}$$

where w is the vertical velocity (cm sec^{-1}) at 500 mb. The above exppression is proportional to the conversion of potential to kinetic energy by transient motions. The field of (1.27) is contoured in Figure 1.6c for CR and in Figure 1.6d for WM. In Fig. 1.6d the intensity index is 40% greater at station A than at station B. However, as we see from Figure 1.6c, the model atmosphere is so noisy that a disparity of more than 20% can be accounted for by chance alone. In summary, it appears that SST anomalies as big as $\pm$ 4 C can influence the pattern of storm intensity if they persist for as long as a year. However, the effect they produce is no more than twice as large as could be expected by chance alone.

Experiment ML developed SST anomalies of about the same magnitude and extent as those observed in Nature. As in the observations (Namias, 1972), the model SST anomalies show good correlation with the atmospheric flow on the scale of quasi-stationary waves

Figure 1.6

A. The variance of potential temperature at 500 mb $\overline{(\theta')^2}$ in CR and

B. in WM; and

C. the transient conversion $\overline{w'\theta'}$ in CR and

D. in WM.
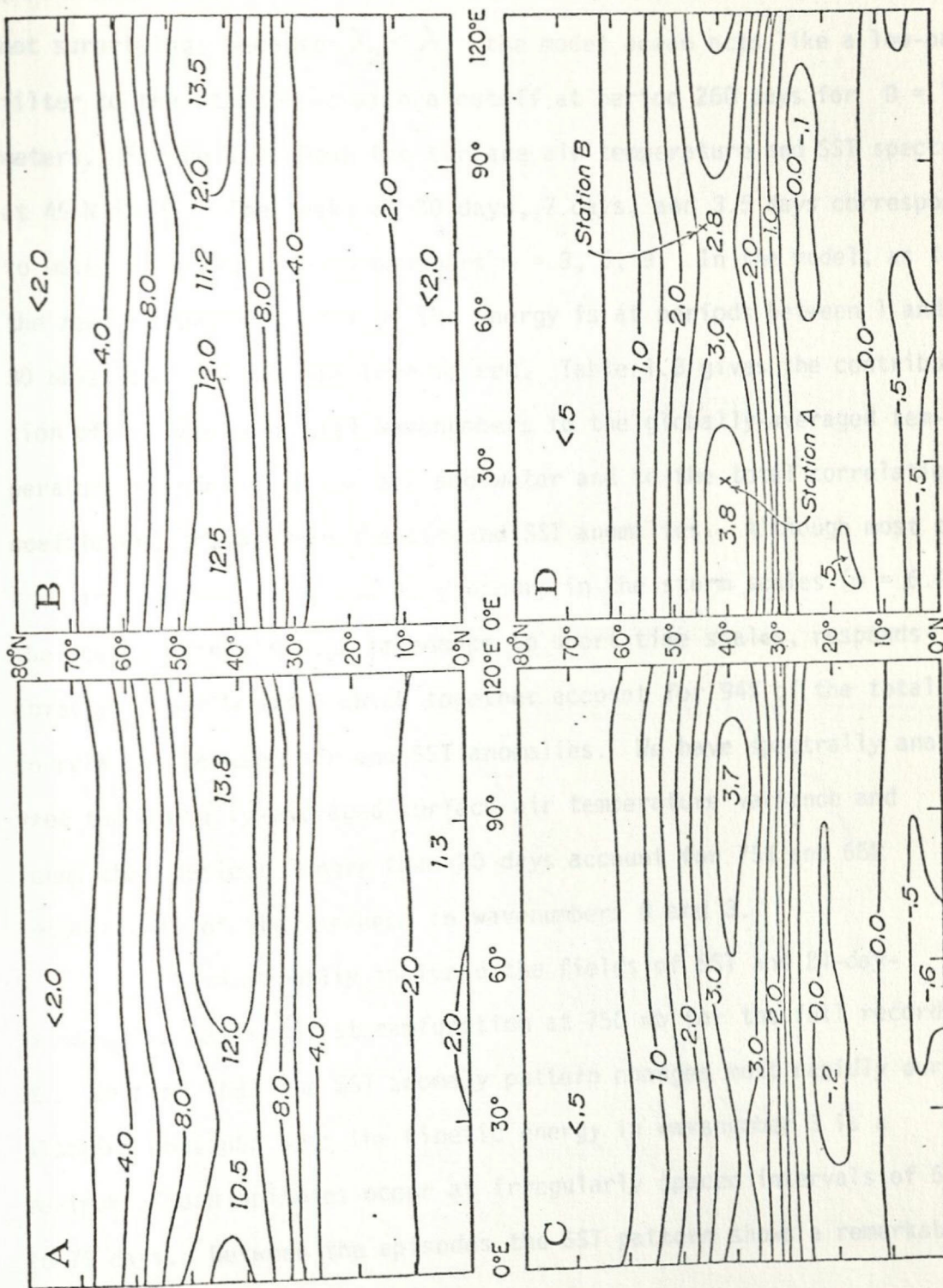
(model wavenumber = 3). In the model at least, this correlation is not surprising; because $\lambda_2 < \lambda_1$ the model ocean acts like a low-pass filter to the atmosphere with a cutoff at period 260 days for D = 10 meters. Figure 1.7 shows the surface air temperature and SST spectra at 45 N in ML. The peaks at 30 days, 7 days, and 3.5 days correspond to waves with discrete wavenumbers m = 3, 6, 9. In the model, as in the real atmosphere, most of the energy is at periods between 1 and 30 days; but the SST spectrum is red. Table 1.3 gives the contribution of the various zonal wavenumbers to the globally-averaged temperature variances in the air and water and to the total correlation coefficient, r, between the air and SST anomalies. Although most of the air temperature variability occurs in the storm scales (m = 6.9), the ocean, with its high impedance to short time scales, responds chiefly to m = 0 and 3 which together account for 94% of the total correlation between air and SST anomalies. We have spectrally analyzed the globally-averaged surface air temperature variance and found that periods longer than 20 days account for 75% and 65% respectively of the variance in wavenumbers 0 and 3.

We have visually analyzed the fields of SST and 24-day-running-mean-averaged streamfunction at 750 mb for the full record in ML. We find that the SST anomaly pattern changes most rapidly during blocking episodes when the kinetic energy in wavenumber 3 is a maximum. Such episodes occur at irregularly spaced intervals of 50 to 75 days. Between the episodes the SST pattern shows a remarkable persistence.
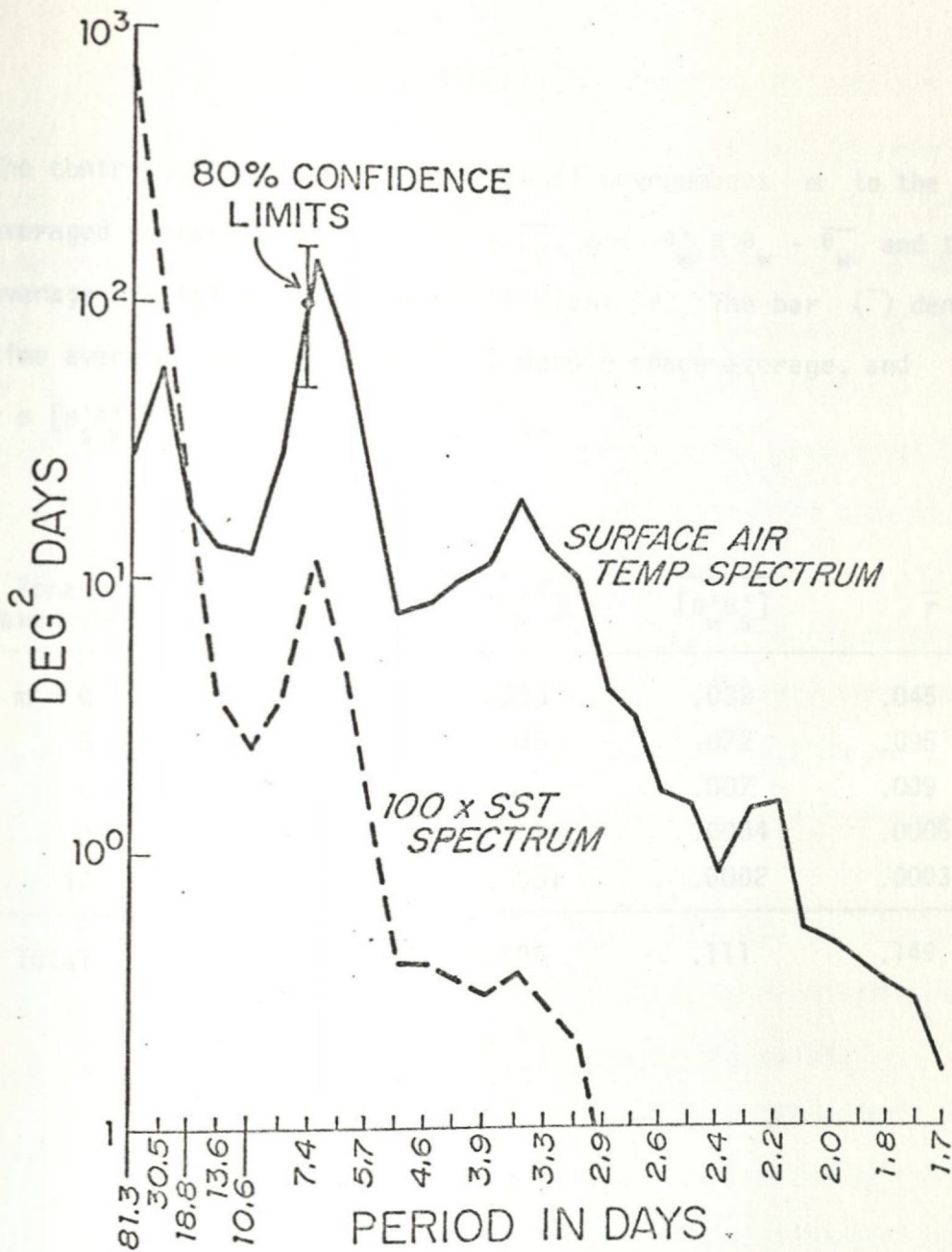
Figure 1.7   Spectra of surface air temperature and 10 x sea
surface temperature at 45 N in ML.   Spectra are
band-averaged over 5 frequencies.

TABLE 1.3

The contribution of the various zonal wavenumbers m to the globally averaged variances of $\theta'_s \equiv \theta_s - \overline{\theta_s}$ and $\theta'_w \equiv \theta_w - \overline{\theta_w}$ and their average spatial correlation coefficient r . The bar $(\overline{})$ denotes time average; the brackets $([\ ])$ denote space average, and

$$r \equiv [\theta'_s \theta'_w] / ([(\theta'_s)^2]^{1/2} [(\theta'_w)^2]^{1/2}).$$

Zonal Wavenumber	$\overline{[(\theta'_s{}^2]}$	$\overline{[(\theta'_w{}^2]}$	$\overline{[\theta'_w \theta'_s]}$	$\overline{r}$
m = 0	.23	.033	.032	.045
3	1.30	.065	.072	.095
6	2.17	.006	.007	.009
9	1.11	.0004	.0004	.0006
12	.57	.0001	.0002	.0003
Total	5.38	.105	.111	.149

In order to determine whether or not the SST anomaly patterns affect the weather in ML we have tried the following procedure: We have computed θ_w from equations (1.14, 1.19) using the surface air temperature θ_s obtained in CR. We refer to the $\theta_w(t)$ so obtained as the "slave ocean" for run CR. In both the slave ocean and the ocean in ML the maximum SST anomalies occur near 50 N. Figure 1.8 shows the longitude, $\varphi_o(t)$, of the maximum (positive) SST anomaly at 50 N for ML and for the slave ocean in CR. In both cases the glob of warm water moves to the east on average.

We now introduce an averaging method which has proved useful in analyzing the slowly moving SST fields. At every time step we determine $\varphi_o(t)$ and translate the picture of the flow until $\varphi_o(t)$ coincides with the zero meridian. The average of all the translated pictures -- which we call the "composite average" -- is the average flow seen by an observer moving with the SST anomaly. We emphasize, however, that all of the quantities so averaged are themselves measured in the reference frame attached to the earth.

Figure 1.9a shows the composite average SST anomaly pattern in ML and the corresponding composite average of the 24-day-running-mean-averaged streamfunction anomaly at 750 mb. As in the real observations (Namias, 1972), warm spots are correlated with anomalous geostrophic wind from the south and high pressure to the east. Figure 1.9b shows the corresponding composite averages for the slave ocean in CR. In Figure 1.9b the SST amplitude and the phase lag between pressure and temperature are smaller than in Figure 1.9a; but
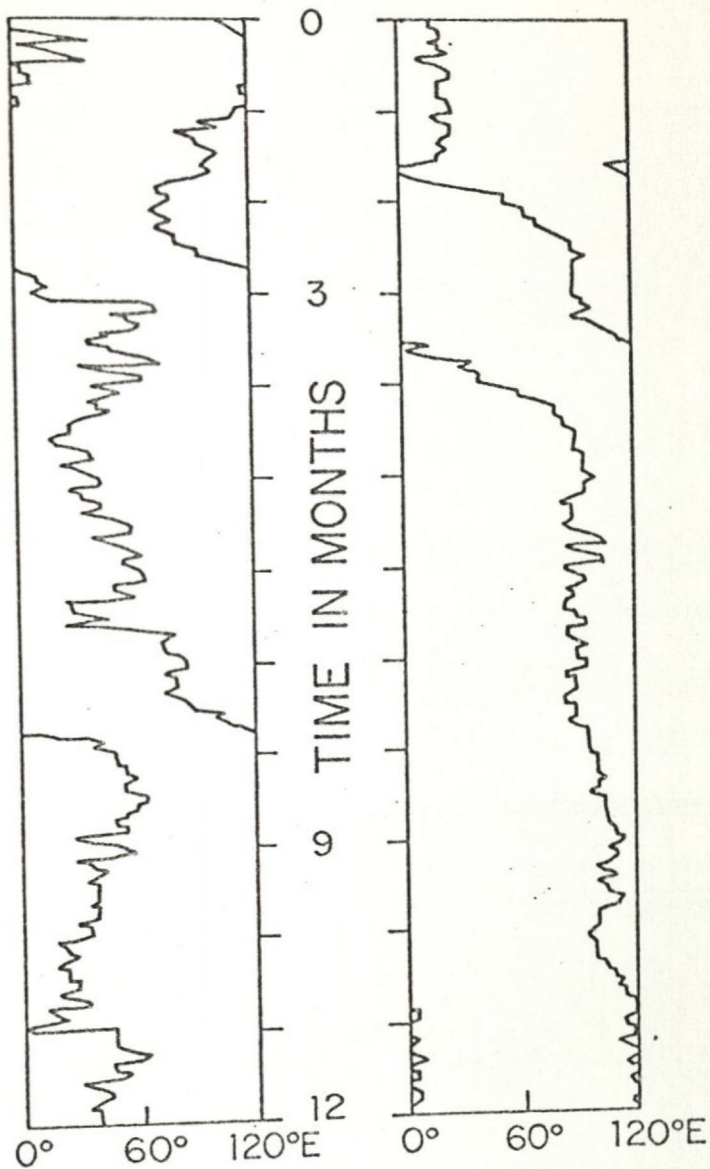
Figure 1.8. The longitude, $\phi_0(t)$, of the maximum positive SST anomaly at 50 N for the slave ocean in CR (left) and for ML (right).

Figure 1.9

A. The composite average SST anomaly (broken line) and 24-day-
    running-mean-averaged streamfunction anomaly at 750 mb for
    ML and

B. for the slave ocean in CR. The Maximum anomalous wind
    speed is 1.6 m-sec^{-1}.

C. The composite average transient conversion (deg-cm-sec^{-1})
    in ML and

D. in CR.
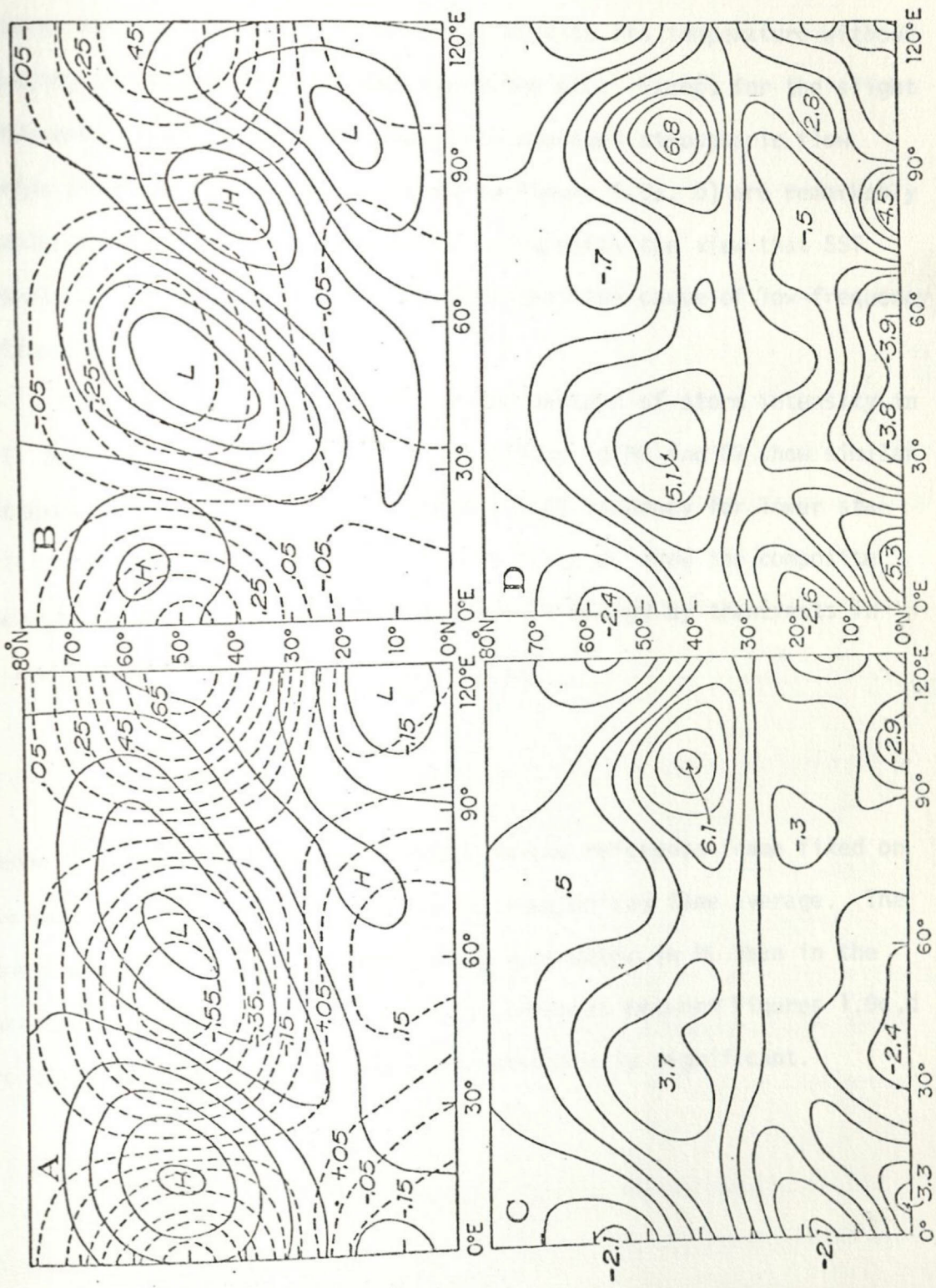
these differences can be quantitatively explained by taking into account the fact that the slave ocean adjusts its temperature without changing the temperature of the overlying air. Except for the slight difference in phase lag, the composite averaged atmospheric flow fields (such as the 750 mb pressure in Figure 1.9a, b) are remarkably similar in ML and CR. This similarity supports the view that SST anomaly patterns are the result rather than the cause of low-frequency motions in the atmosphere.

Do the SST anomalies affect the pattern of storm intensity in ML? The composite average static stability in ML and CR show similar patterns, although there is a slight (.1 C) tendency for lower stability over warm water in ML. Figures 1.9 c,d show the composite average conversion of potential to kinetic energy by transients in ML and in CR. The quantity contoured is:

$$\overline{w\theta}^m - \overline{w}^f\overline{\theta}^f$$

where $(\overline{})^f$ denotes the time average in the reference frame fixed on the earth and $(\overline{})^m$ denotes the moving (composite) time average. The storms are actually less intense over warm water in ML than in the correspoiding location in CR. The differences between Figures 1.9c,d are therefore almost certainly not statistically significant.

4. Discussion

Two quantities are fundamentally important in deciding whether long-term predictions based on sea surface temperature can be useful. The quantities are (in the notation of section 1):

1) the expected change in predictand $\Delta \langle V \rangle$ caused by the anomalous sea state; and

2) the ratio of the expected change to the expected error in the prediction $\Delta \langle V \rangle / \sigma$.

The first quantity determines if and how the predictor (sea temperature) is capable of affecting the statistics of the predictand V. The second quantity measures the confidence that can be placed on a single prediction. In terms of the sea temperature predictability time T_0 and the significance time scale T_s

$$\frac{\Delta \langle V \rangle}{\sigma} \sim 2 \sqrt{\frac{T_0}{T_s}}$$

While any nonzero value of $\Delta \langle V \rangle / \sigma$ represents a definite predictive skill, the present study has shown tha, even for exaggerated SST anomalies where $\Delta \langle V \rangle$ may be appreciable, $\frac{\Delta \langle V \rangle}{\sigma}$ is often small. Whether predictions are ever feasible in such cases will depend largely on the uses to which the predictions will be put. For example, a long-range program of one month agricultural forecasts might be of great ultimate benefit even if the predictions were correct only slightly more often than they were wrong.

The conclusions of this study may depend critically on the many simplifying assumptions we have made, especially our rather

extreme abstraction of the atmospheric heating field in which we explicitly neglect complicated radiation and condensation processes. Even accepting the format of equations (1.15 - 1.19), arguments can no doubt be made that the values of the forcing coefficients should be greater or smaller than the values we have used. Here, we simply restate that our values for the atmospheric friction and heating coefficients were arrived at by the somewhat novel approach of tuning the model to the observed energy cycle. This method may be preferable to a direct estimation of the forcing parameters, because it incorporates the difficulty of allowing for the effect of the infinite vertical diffusion rate within layers upon the average fluxes of momentum and heat. To oceanographers the ten-meter mixed layer will seem too shallow; but we can easily argue that λ should be two or three times the value quoted in section 2, in which case D could be as large as 30 meters with no change in λ_2. More serious, perhaps, is our neglect of ocean currents. In mid-latitudes, at least, anomalous north-south advection of the mean horizontal temperature gradient in the ocean could conceivably compete with anomalous surface heating as the cause of SST anomalies. Finally, by omitting continents, we have neglected important sources of warm and cold air.

However, granting all of the above objections, the results of this study may still be noteworthy both because of the great current interest in air/sea interactions and because the large primitive equation models (which do the best job of simulating climate) cannot yet be run economically enough to answer statistical questions about

what is essentially a statistical problem.

Doos, B. R., 1962. The influence of exchange of sensible heat with [...] the [...] water [...] and the planetary flow. *Tellus*, 14, 133.

Jones, [...] [...] Runge-Kutta-Gauss-dynamo integrals. *Proc. R.* [...]

Lorenz, [...] [...] numerical weather prediction. *Tellus,* [...]

Namias, [...] interactions between North Pacific [...] [...] spheric circulation. *J. Geophys.* [...]

Nam[...] [...] sea surface temperature patterns [...] [...] 70, 511.

[...] [...] interaction between the sea surface and [...] *Oceanogr.*, 3, 329.

[...] [...] atmospheric circulation [...]

[...] [...] atmospheric energetics in the [...] *Space Phys.*, 8, 289.

Smag[...] [...] marginal influence of large-scale heat [...] quasi-stationary mean motions of the [...] *Met. Soc.*, 79, 342.

REFERENCES

Doos, B. R., 1962: The influence of exchange of sensible heat with the earth's surface on the planetary flow. Tellus, 14, 133.

James, R. W., 1973: The Adams and Elsasser dynamo integrals. Proc. R. Soc. Lond., A331, 469.

Lorenz, E. N., 1960: Energy and numerical weather prediction. Tellus, 12, 364.

Namias, J., 1959: Recent seasonal interactions between North Pacific waters and the overlying atmospheric circulation. J. Geophys. Res., 64, 631.

Namias, J., 1972: Space scales of sea-surface temperature patterns and their causes. Fishery Bull., 70, 611.

Namias, J., 1973: Thermal communication between the sea surface and lower troposphere. J. Phys. Oceanogr., 3, 373.

Oort, A. H. and E. M. Rasmusson, 1971: Atmospheric Circulation Statistics. NOAA professional paper 5.

Saltzman, B., 1970: Large scale atmospheric energetics in the wavenumber domain. Rev. Geophys. Space Phys., 8, 289.

Smagorinsky, J., 1953: The dynamical influence of large-scale heat sources and sinks on the quasi-stationary mean motions of the atmosphere. Quart. J. R. Met. Soc., 79, 342.

CHAPTER II

The Equilibrium Statistical Mechanics
of Quasi-geostrophic Flows

Abstract

We have applied the methods of classical statistical mechanics
to derive the inviscid equilibrium states for one- and two-layer
turbulent quasi-geostrophic flows, with and without bottom topography
and variable rotation rate. The mathematical development parallels
that of Khinchin (1949) for systems with a single integral invariant
of the motion. In the one-layer case without topography we recover
the equilibrium energy spectrum given by Kraichnan (1967). In the
two-layer case, we find that the internal radius of deformation con-
stitutes an important dividing scale: At scales of motion larger than
the radius of deformation, the equilibrium flow is nearly barotropic,
while at smaller scales the streamfunctions in the two layers are
statistically uncorrelated. The equilibrium lower layer flow is
positively correlated with bottom topography (anticyclonic flow over
seamounts) and the correlation extends to the upper layer at scales
larger than the radius of deformation. We suggest that some of the
statisitical trends observed in non-equilibrium flows may be looked
on as manifestations of the tendency for turbulent interactions to
maximize the entropy of the system.

1. Introduction

We wish to investigate the equilibrium statistical mechanics of some simple fluid models which are of particular interest to oceanographers and meteorologists. Specifically we shall derive the equilibrium statistical states toward which spectrally-truncated representations of the equations of motion would evolve in the absence of forcing and viscosity. These equilibrium states are of interest in themselves, and may be especially important if realistic non-equilibrium flows are "close" to inviscid equilibrium in some of their properties.

The models considered in this paper are quasi-geostrophic and also quasi-two-dimensional in the sense that they conserve analogs of the kinetic energy and enstrophy of ordinary two-dimensional flow. We focus initially on two complementary systems. The first fluid system consists of a single homogeneous layer bounded vertically by flat horizontal plates. The fluid is constrained by rotation about a vertical axis to move only horizontally so that the governing equation of motion is:

$$\frac{\partial \zeta}{\partial t} + J(\psi, \zeta) = 0 \qquad (2.1)$$

where ψ is the streamfunction of the flow and $\zeta = \nabla^2 \psi$. The equilibrium spectrum associated with (2.1) has been discussed by Kraichnan (1967; 1975); however, a complete mathematical derivation of the equilibrium probability distributions has not appeared in the literature. The derivation presented below follows very closely that

50

of Khinchin (1949) for systems with one integral invariant of the motion. The reasons for presenting it here are two: First, the complete derivation contributes several interesting details to the literature of the statistical mechanics of (2.1); and second, it serves as a model for the mathematically similar but algebraically more complex analysis of the other system introduced below.

The second fluid model corresponds to quasi-geostrophic flow in a system comprised of two immiscible layers. The governing equations are a coupled set:

$$\frac{\partial \mathcal{S}_i}{\partial t} + J(\psi_i, \mathcal{S}_i) \quad , \quad i = 1, 2 \tag{2.2}$$

where ψ_1 is the streamfunction of the top layer, ψ_2 of the bottom layer, and $\mathcal{S}_1$, $\mathcal{S}_2$ are given by:

$$\begin{aligned} \mathcal{S}_1 &= \nabla^2 \psi_1 + F_1(\psi_2 - \psi_1) \\ \mathcal{S}_2 &= \nabla^2 \psi_2 + F_2(\psi_1 - \psi_2) \end{aligned} \tag{2.3}$$

The constants F_1, F_2 are defined by

$$F_i = \frac{f_o^2}{g' D_i}$$

where f_o is twice the (constant) rotation rate, g' the reduced gravity, and D_i the mean depth of the i-th layer. Equations (2.2) express the conservation of the potential vorticity, $\mathcal{S}_i$, of each layer. A detailed derivation of these equations is given by Pedlosky

(1970). With a slightly different interpretation on the F_i, equations (2.2 - 2.3) are equivalent to the "two-and-one-half-level baroclinic Model" of the atmosphere (see, for example, Phillips (1956)). The equilibrium state of (2.2) has not been previously discussed.

Both the systems (2.1) and (2.2) have been used to model geophysical flows. They differ from the general quasi-geostrophic equations in their neglect of the spatial variation of f_o and D_i. We defer discussion of these latter effects until later in this paper. The initial goal is to contrast the equilibrium states of (2.1) and (2.2), or, said another way, to study (2.2) under the discontinuous cases $F_i = 0$, $F_i \neq 0$.

Both the systems (2.1) and (2.2) are assumed to have simple closed horizontal boundaries. Corresponding to these boundaries we define eigenfunctions $\{\varphi_i\}$ as the solutions to:

$$(2.4)$$

$$\begin{cases} \nabla^2 \varphi_i = -k_i^2 \varphi_i \ , & k_i^2 > 0 \quad \text{constant} \\ \\ \varphi_i = 0 & \text{on the boundary} \end{cases}$$

with normalization $\overline{\varphi_i^2} = 1$, where the overbar denotes integration over the region enclosed by the boundaries. For simplicity we assume $k_i^2 \neq k_j^2$ when $i \neq j$. (when this condition fails in practice it can always be restored by infinitesimal perturbations in the boundaries.) It then follows that $\overline{\varphi_i \varphi_j} = \delta_{ij}$. The functions $\{\varphi_i\}$ are assumed to be complete in the sense that for any regular function $f(x,y)$

$$f = \sum_{i=1}^{\infty} f_i \, \varphi_i(x,y) \quad ; \quad f_i = \overline{f \varphi_i}$$

except perhaps at boundary points. We then expand the dependent

variables of (2.1) and (2.2) in terms of the eigenfunctions:

$$\psi = \sum_{i=1}^{\infty} \frac{x_i}{k_i} \, \varphi_i \tag{2.5}$$

$$(\psi_1, \psi_2) = \sum_{i=1}^{\infty} (a_i, b_i) \, \varphi_i$$

The choice of notation is a matter of convenience.

The coefficients $\{x_i\}$ and $\{a_i, b_i\}$ comprise generalized

coordinates for the systems (2.1) and (2.2). In the phase spaces

spanned by these coordinates each point represents a possible state

of the fluid system, and the evolution of the fluid system is describ-

ed by a trajectory that is specified by (2.1) and (2.2) in the form:

$$\tag{2.6}$$

$$\frac{dx_i}{dt} = \sum_{j} \sum_{\ell} \frac{k_\ell^2}{k_i k_j k_\ell} \, \beta_{ij\ell} \, x_j x_\ell$$

$$\frac{dA_i}{dt} = \sum_{j} \sum_{\ell} \beta_{ij\ell} \, a_j A_\ell \quad ; \quad A_i \equiv -(k_i^2 + F_1) a_i + F_1 b_i$$

$$\frac{dB_i}{dt} = \sum_{j} \sum_{\ell} \beta_{ij\ell} \, b_j B_\ell \quad ; \quad B_i \equiv -(k_i^2 + F_2) b_i + F_2 a_i$$

where

$$\beta_{ij\ell} = -\overline{\varphi_i \, J(\varphi_j, \varphi_\ell)}$$

Let $\mathcal{P}(x_1, x_2, \ldots, x_n, t)$ and $\mathcal{P}(a_1, \ldots, a_n, b_1, \ldots, b_n, t)$ be the probability distribution functions for states in the phase spaces, which we now assume to be <u>finite-dimensional</u>. The time evolution of the finite-dimensional systems is assumed to be governed by (2.6) with the summations truncated to run from 1 up to n. By definition, the probability functions obey Liouville's equation:

$$\frac{\partial}{\partial t} \mathcal{P} + \sum_{i=1}^{n} \frac{\partial}{\partial x_i} (\mathcal{P} \dot{x}_i) \tag{2.7}$$

and a similar equation for the other system. Equation (2.7) may be thought of as a continuity equation for motion in phase space with the "velocity" $\dot{x}_i$ given by (2.6). From (2.6) and the fact that β_{ijl} is zero whenever two of its indices are equal, it follows that

$\frac{\partial \dot{x}_i}{\partial x_i} = 0$ so that (2.7) becomes:

$$\frac{\partial \mathcal{P}}{\partial t} + \sum_{i=1}^{n} \dot{x}_i \frac{\partial \mathcal{P}}{\partial x_i} \equiv \frac{D\mathcal{P}}{Dt} = 0 \tag{2.8}$$

At equilibrium ($\frac{\partial \mathcal{P}}{\partial t} = 0$), $\mathcal{P}(x_1, x_2, \ldots, x_n)$ is constant along trajectories in phase space. If a trajectory eventually passes arbitrarily close to every point within a given volume V of phase space, then it follows from (2.8) that $\mathcal{P}$ is a constant over V. The conventional assumption of equal <u>a priori</u> probability distribution in phase space is then equivalent to the assumption that V is determined only by a few general constraints on the motion.

System (2.1) conserves the quantities $\overline{\nabla\psi\cdot\nabla\psi}$ and $\overline{\varsigma^n}$ where n is any integer. However, the spectrally-truncated form of

(2.6) conserves only the spectrally-truncated forms of $\nabla\psi\cdot\nabla\psi$ and ψ^2 and we take these for our general integral invariants. Similar remarks apply to system (2.2) with quadratic invariants $\overline{\psi_1^2}$, $\overline{\psi_2^2}$ and $\overline{\dfrac{\nabla\psi_1\cdot\nabla\psi_1}{F_1} + \dfrac{\nabla\psi_2\cdot\nabla\psi_2}{F_2} + (\psi_1 - \psi_2)^2}$. In terms of the generalized Fourier coefficients the constraints are:

$$\sum_{i=1}^{n} x_i^2 = E \qquad\qquad \sum_{i=1}^{n} k_i^2 x_i^2 = Z \qquad\qquad (2.9)$$

where E and Z are constants proportional to the kinetic energy and enstrophy; and

$$\sum_{i=1}^{n} A_i^2 = Z_a \qquad\qquad (2.10)$$

$$\sum_{i=1}^{n} B_i^2 = Z_b$$

$$\sum_{i=1}^{n} C_i^2 = \sum_{i=1}^{n} \frac{\dfrac{(k_i^2 + F_2)}{F_1} A_i^2 + \dfrac{(k_i^2 + F_1)}{F_2} B_i^2 + 2 A_i B_i}{k_i^2 (k_i^2 + F_1 + F_2)} = E_{ab}$$

where Z_a, Z_b, and E_{ab} correspond to the potential enstrophies in the top and bottom layer and to the sum of total kinetic and available potential energy.

We note in passing the existence of an alternative mathematical formulation. In place of the truncated-spectral streamfunction representation adopted here, one might instead consider the flow to be comprised of a large but finite number of discrete point vortices. Liouville's theorem applies to the latter system if the phase coordinates are taken to be the Cartesian coordinates of each vortex center. The statistical mechanics of the discrete vortex system was

56

first discussed by Onsager (1949) and an extensive literature exists.
However, for the present application we much prefer the spectral
formulation as the superior approximation to continuum fluid flow.

2. The Single-layer System

Corresponding to system (2.1), let $x_1, x_2, \ldots, x_n$ be the coordinates of an n-dimensional phase space which we denote by Γ. Let

$$E(x_1, x_2, \ldots, x_n) = x_1^2 + x_2^2 + \ldots + x_n^2$$

and

$$Z(x_1, x_2, \ldots, x_n) = k_1^2 x_1^2 + k_2^2 x_2^2 + \ldots + k_n^2 x_n^2$$

be phase functions which we refer to as energy and enstrophy. Any set of coordinates (not including all n coordinates) will be called a component of the system. The subspace consisting of the coordinates of a particular component j will be denoted by Γ_j. The smallest component subspace is one that contains only a single coordinate x_r and we denote it by the special symbol γ_r.

We define the structure function of the system by:

$$(2.11)$$

$$\Omega(E, Z) = \lim_{\delta E, \delta Z \to 0} \frac{1}{\delta E \cdot \delta Z} \iiiint dV$$

$$E - \frac{\delta E}{2} < \sum_i x_i^2 < E + \frac{\delta E}{2}$$

$$Z - \frac{\delta Z}{2} < \sum_i k_i^2 x_i^2 < Z + \frac{\delta Z}{2}$$

where $dV = dx_1\, dx_2 \ldots dx_n$ is a volume element in Γ. Thus $\Omega(E,Z)dEdZ$ is the volume of phase space Γ in which the energy is within $\frac{dE}{2}$ of E and the enstrophy within $\frac{dZ}{2}$ of Z. If $f(x_1, \ldots, x_n)$ is any phase function, then the phase average of f in

a system with energy E and enstrophy Z is assumed to be

$$\langle f \rangle = \lim_{\delta E, \delta Z \to 0} \frac{1}{\delta E \cdot \delta Z} \frac{1}{\Omega(E,Z)} \iiint f \, dV \qquad (2.12)$$

where the integration limits are the same as in (2.11). For any
component we define the component structure function $\Omega_j(E,Z)$ by an
integral similar to (2.11), but with dV replaced by dV_j, a
volume element in Γ_j, and the integration performed only over the
region of Γ_j in which the energy of the component is within $\frac{\delta E}{2}$
of E and the enstrophy within $\frac{\delta Z}{2}$ of Z. It can easily be shown
(Appendix A) that if the full system consists of m components
(m $\leqslant$ n) with no coordinates in common then

$$\Omega(E,Z) = \iiint \left[\prod_{i=1}^{m-1} dE_i \, dZ_i \, \Omega_i(E_i, Z_i) \right] \times \qquad (2.13)$$
$$\times \, \Omega_m \left(E - \sum_{i=1}^{m-1} E_i, \, Z - \sum_{i=1}^{m-1} Z_i \right)$$

Thus the structure functions obey a composition law analagous to
convolution.

   Knowledge of the structure functions gives information about
the probability distributions of the components. Consider a system
comprised of two components with subspaces Γ_1 and Γ_2. Every
state of the system, represented by a point P in Γ determines a
corresponding point P_1 in Γ_1. In Appendix A it is shown that the
probability distribution function for P_1 in its Γ_1 subspace is
given by

$$\frac{\Omega_2(E-E_1, Z-Z_1)}{\Omega(E,Z)} \tag{2.14}$$

where E and Z are the constant energy and enstrophy of the entire system; E_1 and Z_1 the energy and enstrophy of component 1, which vary with position in Γ_1; and Ω_2 is the structure function of component 2.

We begin the analysis by calculating the structure function for a component consisting of a single coordinate x_i. It is by definition:

$$\omega_i(E,Z) = \lim_{\delta E, \delta Z \to 0} \frac{1}{\delta E \cdot \delta Z} \int_{\substack{E-\frac{\delta E}{2}<x_i^2<E+\frac{\delta E}{2} \\ Z-\frac{\delta Z}{2}<k_i^2 x_i^2<Z+\frac{\delta Z}{2}}} dx_i$$

which is infinite for $k_i^2 E = Z$ and zero otherwise. We set

$$\omega_i(E,Z) = \mathcal{C}(k_i,E)\,\delta(k_i^2 E-Z)$$

where $\mathcal{C}(k_i,E)$ has to be determined. Integrating the above relation one finds that

$$\mathcal{C}(k_i,E) = \int_0^\infty \omega_i(E,Z)\,dZ \quad \text{for } E, Z>0$$

However,

$$\int_0^\infty \omega_i(E,Z)\,dZ = \lim_{\delta E \to 0} \frac{1}{\delta E}\int_{E-\frac{\delta E}{2}<x_i^2<E+\frac{\delta E}{2}} dx_i = \frac{1}{\sqrt{E}}$$

and thus

$$\omega_i(E,Z) = \frac{1}{\sqrt{E}}\,\delta(k_i^2 E-Z) \quad \text{for } E,Z>0. \tag{2.15}$$

One can now, in principle, compute the structure function of a component consisting of any number of coordinates simply by using (2.15) in the general formula (2.13). However, for components containing a large number of coordinates the integration in (2.13) becomes difficult and we seek an asymptotic result. Following Khinchin, we define the generating functions and conjugate functions for the system and its components:

$$\Phi(\alpha, \beta) = \int_0^\infty dE \int_0^\infty dZ \, \Omega(E, Z) e^{-\alpha E - \beta Z} \qquad (2.16)$$

$$U^{(\alpha, \beta)}(E, Z) = e^{-\alpha E - \beta Z} \Omega(E, Z) / \Phi(\alpha, \beta)$$

$$\Phi_i(\alpha, \beta) = \int_0^\infty dE \int_0^\infty dZ \, \Omega_i(E, Z) e^{-\alpha E - \beta Z}$$

$$U_i^{(\alpha, \beta)}(E, Z) = e^{-\alpha E - \beta Z} \Omega_i(E, Z) / \Phi_i(\alpha, \beta)$$

Here, α and β are any two real numbers for which the integrals converge. From equation (2.13) it can easily be shown that

$$\Phi(\alpha, \beta) = \prod_{i=1}^{m} \Phi_i(\alpha, \beta) \qquad (2.17)$$

and

$$U^{(\alpha,\beta)}(E,Z) = \iiint \left[\prod_{i=1}^{m-1} dE_i\, dZ_i\; U_i^{(\alpha,\beta)}(E_i,Z_i) \right] \times \qquad (2.18)$$

$$\times\; U_m^{(\alpha,\beta)}\left(E - \sum_{i=1}^{m-1} E_i,\; Z - \sum_{i=1}^{m-1} Z_i\right)$$

That is, the conjugate functions obey the same composition law as the structure functions. However, the conjugate functions are integrable:

$$\int_0^\infty dE \int_0^\infty dZ\; U_i^{(\alpha,\beta)}(E,Z) = 1$$

whereas the structure functions are in general not integrable.

The expression (2.18) can be <u>looked on</u> as the joint probability distribution of the sums of independent random variables

$$E = E_1 + E_2 + \ldots + E_m$$

$$Z = Z_1 + Z_2 + \ldots + Z_m$$

expressed in terms of the joint distribution functions of E_i and Z_i.[1] If the $U_i^{(\alpha,\beta)}(E,Z)$ satisfy the conditions of the Central Limit Theorem, then as $m \to \infty$, the expression (2.18) tneds asymptotically to:

$$(2.19)$$

$$U^{(\alpha,\beta)}(E,Z) \sim \frac{1}{2\pi\, \sigma_E\, \sigma_Z \sqrt{1-\rho^2}}\; \exp\left\{ -\frac{1}{2(1-\rho^2)} \times \right.$$

$$\left. \times \left[\left(\frac{E-m_E}{\sigma_E}\right)^2 - 2\rho\left(\frac{E-m_E}{\sigma_E}\right)\left(\frac{Z-m_Z}{\sigma_Z}\right) + \left(\frac{Z-m_Z}{\sigma_Z}\right)^2 \right] \right\}$$

---

[1] It will turn out that, for a suitable choice of α and β, the $U_i^{(\alpha,\beta)}(E,Z)$ are joint distribution functions for the energy and enstrophy of the components.

where

$$m_E = \sum_{i=1}^{m} m_{E_i} \qquad m_{E_i} = \int\int_0^\infty E U_i^{(\alpha,\beta)}(E,Z)\,dE\,dZ \qquad (2.20)$$

$$\sigma_E^2 = \sum_{i=1}^{m} \sigma_{E_i}^2 \qquad \sigma_{E_i}^2 = \int\int_0^\infty (E - m_{E_i})^2 U_i^{(\alpha,\beta)}(E,Z)\,dE\,dZ$$

$$\rho = \frac{1}{\sigma_E \sigma_Z}\sum_{i=1}^{m}\rho_i \qquad \rho_i = \int\int_0^\infty (E - m_{E_i})(Z - m_{Z_i})U_i^{(\alpha,\beta)}(E,Z)\,dE\,dZ$$

and similarly for m_Z and σ_Z^2. By means of (2.16) we may express the above parameters in terms of the generating functions:

$$(2.21)$$

$$m_E = -[\ln \Phi]_\alpha \qquad m_Z = -[\ln \Phi]_\beta$$

$$\sigma_E^2 = [\ln \Phi]_{\alpha\alpha} \qquad \sigma_Z^2 = [\ln \Phi]_{\beta\beta}$$

$$\rho = [\ln \Phi]_{\alpha\beta}\Big/\sqrt{[\ln \Phi]_{\alpha\alpha}[\ln \Phi]_{\beta\beta}}$$

Now consider the problem of obtaining an expression for the distribution of the phase point corresponding to the state of a small component (i.e. one containing few coordinates) in its component subspace in the case where the total phase space has a very large dimension. Let Ω be the structure function for the entire system, Ω_1, the structure function for the small component, and Ω_2 the structure function for the component with subspace $\Gamma_2' = \Gamma - \Gamma_1$. The exact expression for the function we seek is then given by (2.14) with E and Z equal to the total energy and enstrophy of the

system. Since both Γ and Γ_2 contain a large number of coordinates, we can use the asymptotic expression (2.19) for both Ω and Ω_2. The constants α and β have so far been arbitrary, but we now find it convenient to define them to be the roots of the two coupled equations:

$$E = -\frac{\partial}{\partial \alpha} \ln \underline{\Phi}(\alpha, \beta) \qquad (2.22)$$

$$Z = -\frac{\partial}{\partial \beta} \ln \underline{\Phi}(\alpha, \beta)$$

At this point we assume these solutions exist in which case it is obvious that the integrals in (2.16) converge. Then using (2.19 - 2.22) we obtain, after some simplification, the following asymptotic expression for

$$(2.23)$$

$$\frac{\Omega_2(E-E_1, Z-Z_1)}{\Omega(E, Z)} \sim \frac{A}{\Phi(\alpha, \beta)} \exp\left[-\alpha E_1 - \beta Z_1 - B(E_1 - m_{E_1})^2 + C(E - m_{E_1})(Z - m_{Z_1}) - D(Z_1 - m_{Z_1})^2\right]$$

where A, B, C, D are constants given by

$$A = \sqrt{\frac{S(\underline{\Phi})}{S(\underline{\Phi}_2)}} \qquad B = \frac{1}{2} \frac{(\ln \underline{\Phi}_2)_{\beta\beta}}{S(\underline{\Phi}_2)} \qquad C = \frac{(\ln \underline{\Phi}_2)_{\alpha\beta}}{S(\underline{\Phi}_2)} \qquad D = \frac{1}{2} \frac{(\ln \underline{\Phi}_2)_{\alpha\alpha}}{S(\underline{\Phi}_2)}$$

and

$$S(\underline{\Phi}) = (\ln \underline{\Phi})_{\alpha\alpha}(\ln \underline{\Phi})_{\beta\beta} - \left[(\ln \underline{\Phi})_{\alpha\beta}\right]^2 .$$

If the last three terms in the exponent in (2.23) are negligible then (2.23) reduces to Boltzmann's Law.

We can now apply (2.23) to find the probability distribution of a single coordinate x_i in system (2.1). Putting (2.15) into (2.16) we obtain for the generating function of the component consisting of x_i:

$$\phi_i(\alpha, \beta) = \sqrt{\frac{\pi}{\alpha + \beta k_i^2}} \tag{2.24}$$

provided $\alpha + \beta k_i^2 > 0$. (If not, then ϕ_i is divergent.) According to (2.22), α and β are the solutions to the equations:

$$\tag{2.25}$$

$$E = \frac{1}{2} \sum_{i=1}^{n} \frac{1}{\alpha + \beta k_i^2}$$

$$Z = \frac{1}{2} \sum_{i=1}^{n} \frac{k_i^2}{\alpha + \beta k_i^2}$$

In Appendix B we show that such solutions exist and are unique for any E and $Z = k_*^2 E$ provided $k_{min}^2 \leq k_*^2 \leq k_{max}^2$ where k_{min}^2 and k_{max}^2 are the minimum and maximum squared wavenumbers in the truncation. This result is a generalization of a theorem of Fox and Orszag (1973). Using (2.24) in (2.23) we obtain the distribution function for x_i:

$$f_i(x_i) = \sqrt{\frac{\alpha + \beta k_i^2}{\pi}} A_i e^{-(\alpha + \beta k_i^2)x_i^2 - F_i \left(x_i^2 - \frac{1}{2} \frac{1}{\alpha + \beta k_i^2}\right)^2} \tag{2.26}$$

where

$$A_i = \sqrt{1 + G_i} \qquad F_i = (\alpha + \beta k_i^2)^2 G_i$$

and

$$G_i = 2 \sum_\ell \frac{(k_\ell^2 - k_i^2)^2}{(\alpha + \beta k_\ell^2)^2 (\alpha + \beta k_i^2)^2} \bigg/ \sum_{\ell \neq i} \sum_{j \neq i} \frac{(k_\ell^2 - k_j^2)^2}{(\alpha + \beta k_\ell^2)^2 (\alpha + \beta k_j^2)^2}$$

For small G_i, x_i is normally distributed with expected energy

$$\langle E_i \rangle \equiv \langle x_i^2 \rangle = \frac{1}{2} \frac{1}{\alpha + \beta k_i^2} \tag{2.27}$$

When G_i is not small (which is the case when mode i contains an appreciable fraction of the total energy) then the distribution function for x_i contains a significant correction in the form of local maxima at the rms x_i. For modes evenly distributed in wavenumber space, equation (2.27) predicts an equilibrium energy spectrum of general form

$$E(k) = \frac{k}{a + bk^2} \tag{2.28}$$

which can range between ± 1 in slope. Thus equilibrium statistical mechanics predicts a spectral power law that is in rather poor agreement with the inertial ranges of two-dimensional turbulence which are thought to be $k^{-5/3}$ and k^{-3}. Equation (2.28) has been verified in numerical simulations of (2.1) by Fox and Orszag (1973) and Basdevant and Sadourny (1975).

It is interesting to note that the equilibrium circulation $\overline{\mathcal{J}}$ is zero for our truncated system. This is in contrast to the

untruncated equations for which $\bar{\mathcal{F}}$ is conserved (and thus nonzero in general) and it suggests that not all of our results will generalize to numerical schemes that conserve the analog of $\bar{\mathcal{F}}$ as well as $\overline{\mathcal{F}^2}$ and $\overline{\nabla\psi\cdot\nabla\psi}$.

$$\tag{2.29}$$

$$\tag{2.30}$$

3. The Two-layer System

We consider now the baroclinic system (2.2) with integral invariants given by (2.5). The mathematical development parallels the single-layer case rather closely, and we present only the results. In the two-layer system the smallest component with definable energy and potential enstrophies consists of $\underline{two}$ coordinates a_i and b_i, and the Boltzmann Law approximation to their joint probability distribution is found to be:

$$\mathcal{P}_i(a_i, b_i) = \frac{\sqrt{Q_i R_i - P_i^2}}{\pi} \exp\left[-Q_i a_i^2 - R_i b_i^2 + 2P_i a_i b_i\right] \tag{2.29}$$

where

$$Q_i = \alpha(r_i + 1) + \beta_1(r_i + 1)^2 + \beta_2$$
$$R_i = \alpha\left(\frac{r_i}{\delta} + 1\right) + \beta_1 + \beta_2\left(\frac{r_i}{\delta} + 1\right)^2$$
$$P_i = \alpha + \beta_1(r_i + 1) + \beta_2\left(\frac{r_i}{\delta} + 1\right)$$

and $r_i = k_i^2/F_1$ is the nondimensional square wavenumber, $\delta = D_1/D_2$, and α, β_1, β_2 are constants that depend on the specified total energy and potential enstrophies of the system. The conditions on α, β_1, β_2 for the existence of the generating functions $\phi_i(\alpha, \beta_1, \beta_2)$ are the same as the conditions for the integrability of $\mathcal{P}_i(a_i, b_i)$, namely:

$$Q_i > 0 \quad \text{or} \quad R_i > 0 \tag{2.30}$$

and

$$Q_i R_i - P_i^2 = \frac{r}{\delta}(r+1+\delta)\left[\alpha^2 + \beta_1\beta_2\frac{r}{\delta}(r+1+\delta)+\right.$$

$$\left. + \alpha\beta_1(r+1) + \alpha\beta_2\left(\frac{r}{\delta}+1\right)\right] > 0$$

for every i. For given values of the constants of motion E_{ab}, Z_a, Z_b we find α, β_1, β_2 as the solutions to the equations:

$$\sum_i \langle E_{ab_i}\rangle = E_{ab} \tag{2.31}$$

$$\sum_i \langle Z_{a_i}\rangle = Z_a$$

$$\sum_i \langle Z_{b_i}\rangle = Z_b$$

subject to the conditions (2.30). Equations (2.31) are the analogs of (2.25) in the single-layer case.

From (2.29) one may readily compute

$$\tag{2.32}$$

$$\langle a_i^2\rangle = R_i/2\,(Q_i R_i - P_i^2)$$

$$\langle b_i^2\rangle = Q_i/2\,(Q_i R_i - P_i^2)$$

$$\langle a_i b_i\rangle = P_i/2\,(Q_i R_i - P_i^2)$$

and thereby obtain expressions for the following quantities of physical interest:

(i) the average kinetic energy per unit depth in mode i

in the top layer $\quad K_T = 1/2 \, k_i^2 \, \langle a_i^2 \rangle$

in the bottom layer $\quad K_T = 1/2 \, k_i^2 \, \langle b_i^2 \rangle$

(ii) the average available potential energy in mode i $\dfrac{f_o^{-2}}{2g'} \langle (a_i - b_i)^2 \rangle$

and its ratio to the total kinetic energy

(iii) the correlation coefficient $P_i = \langle a_i b_i \rangle / \sqrt{\langle a_i^2 \, b_i^2 \rangle}$ between

the streamfunctions in the top and bottom layer in mode i.

We note that if our truncated system contains arbitrarily large wavenumbers $(k_{max}^2 \to \infty)$ then the conditions that Q_i, $R_i > 0$ restrict β_1, β_2 to positive values. In this circumstance it can easily be shown that P_i assumes only positive values so that the streamfunctions in the two layers are positively correlated at all wavenumbers. If β_i, $\beta_2 < 0$ then the layers may be negatively correlated. Such states are artificial in the sense that they exist only because of the finite truncation. They represent the relaxation states for fluids in which the energy is initially peaked near k_{max}. As the system adjusts toward equilibrium, energy spreads toward lower wavenumbers, decreasing the enstrophy, and forcing a negative correlation between layers to conserve potential enstrophy. For flow in bounded domains $(k_{min}^2 > 0)$ equilibrium states in which $\alpha < 0$ are possible. These states are non-artificial in the sense that boundedness is a property of real flows, but they show no discontinuous change in any property from equilibrium states in which $\alpha > 0$. For systems containing arbitrarily large and small scales, the conditions

(2.30) become α, β_1, $\beta_2 > 0$.

We delete the subscript from r_i and regard r as a continuously varying nondimensional square wavenumber with the value $r = 1 + \delta$ corresponding to motion at the internal Rossby radius of deformation. In the two-layer system, the radius of deformation constitutes an important dividing scale. At scales of motion large compared to $r = 1, \delta$ the kinetic energy spectra (per unit depth) of the two layers are nearly equal and assume the same general form as the equilibrium spectrum (2.28) for a single-layer flow:

$$r^{1/2} K_T \propto \frac{r^{1/2}}{\left[\alpha + \frac{\beta_1 \beta_2}{(\alpha + \beta_1 + \beta_2)} \frac{(1+\delta)}{\delta} r \right]} \quad \text{for } r \ll 1, \delta \tag{2.33}$$

The kinetic energy spectra also approach the single-layer limit at sufficiently small scales:

$$r^{1/2} K_T \propto \frac{r^{1/2}}{\alpha + \beta_1 r} \left[1 + \frac{\delta \beta_1}{r(\alpha + \beta_2 r/\delta)} \right] \tag{2.34}$$

$$r^{1/2} K_B \propto \frac{\delta r^{1/2}}{\alpha + \beta_2 r/\delta} \left[1 + \frac{\beta_2}{r(\alpha + \beta_1 r)} \right]$$

$$\text{for } r \gg 1 + \delta$$

As r becomes large, their ratio, top to bottom, tends to the value $\mathcal{R}^\infty = \beta_2 / \beta_1 \delta^2$. The available potential energy spectrum approaches zero at either extreme. For $r \ll 1, \delta$ the correlation coefficient between layers is nearly unity, but it falls abruptly toward zero near where r equals the larger of $\delta \sqrt{\mathcal{R}^\infty}$ and $1/\sqrt{\mathcal{R}^\infty}$. In cases of interest the latter expressions are both of

order unity. Thus equilibrium two-layer flow resembles a single
barotropic layer on scales larger than the radius of deformation and
two uncorrelated single layers on smaller scales.

If $\delta = 1$ and $\beta = \beta_1 = \beta_2$ then we are examining the
algebraically simple case of "equivalent layers". If $\beta > 0$ then the
realizability conditions (2.30) become simply $\alpha > -\beta r_{min}$. Assume
$r_{min} \ll 1$ and $r_{max} \gg 1$. The two kinetic energy spectra are
identical and their shape is controlled by the ratio β/α. If
$0 < \frac{\beta}{\alpha} < 1/r_{max}$ then the spectra are increasing with r at all
wavenumbers, but if $|\frac{\beta}{\alpha}| > 1/rmin \gg 1$ the spectra are red. For
$\frac{1}{r_{max}} < \frac{\beta}{\alpha} < \frac{1}{r_{min}}$ the spectra have a maximum between r_{min} and r_{max}.
The ratio of available potential to total kinetic energy is:

$$\frac{1}{(1+r) + \frac{\beta(r+2)}{\alpha + \beta r}} < 1$$

which peaks near $r = \sqrt{2}$ at a value of .24 for $|\frac{\beta}{\alpha}| \gg 1$.

The ocean and atmosphere are stongly forced fluids whose
high-wavenumber cut-offs are not arbitrarily-chosen limits, but are
determined by the "viscosity" itself. Nevertheless, the model
equations (2.2) contain realistic turbulent interaction terms, and we
may expect even stron_ly viscous flow to exhibit some of the character-
istics of the model inviscid equilibrium if the turbulent interactions
are efficient in moving the system toward the state of maximum entropy.
In any case, the equilibrium states should indicate the direction in
which the interactions will tend to drive the statistics of real flows.

Figure 2.1 presents the equilibrium statistical variables in model two-layer fluids corresponding to the ocean and atmosphere. We choose $\delta = 1/7$ for the ocean and $\delta = 1$ for the troposphere. The "inverse temperatures" α, β_1, β_2 are chosen to make $\mathcal{R}^\infty = 10$, and the ratios $\frac{\beta_1}{\alpha}$ and $\frac{\beta_2}{\alpha}$ are near the minimum required to make the kinetic energy spectra red at $r_{min} = 10^{-3}$.

Figure 2.1a

The kinetic energy spectra per unit depth (solid lines, arbitrary scale) and the available potential energy spectrum (dashed line, different arbitrary scale) for equilibrium two layer flow in the case where $\delta = 1/7, \mathcal{R}^{\infty} = 10$, and $\beta_1/\alpha = 10^3$. The kilometer scale gives the corresponding inverse wavenumber in an ocean with a radius of deformation of 35 km, the value on earth in mid-latitude.
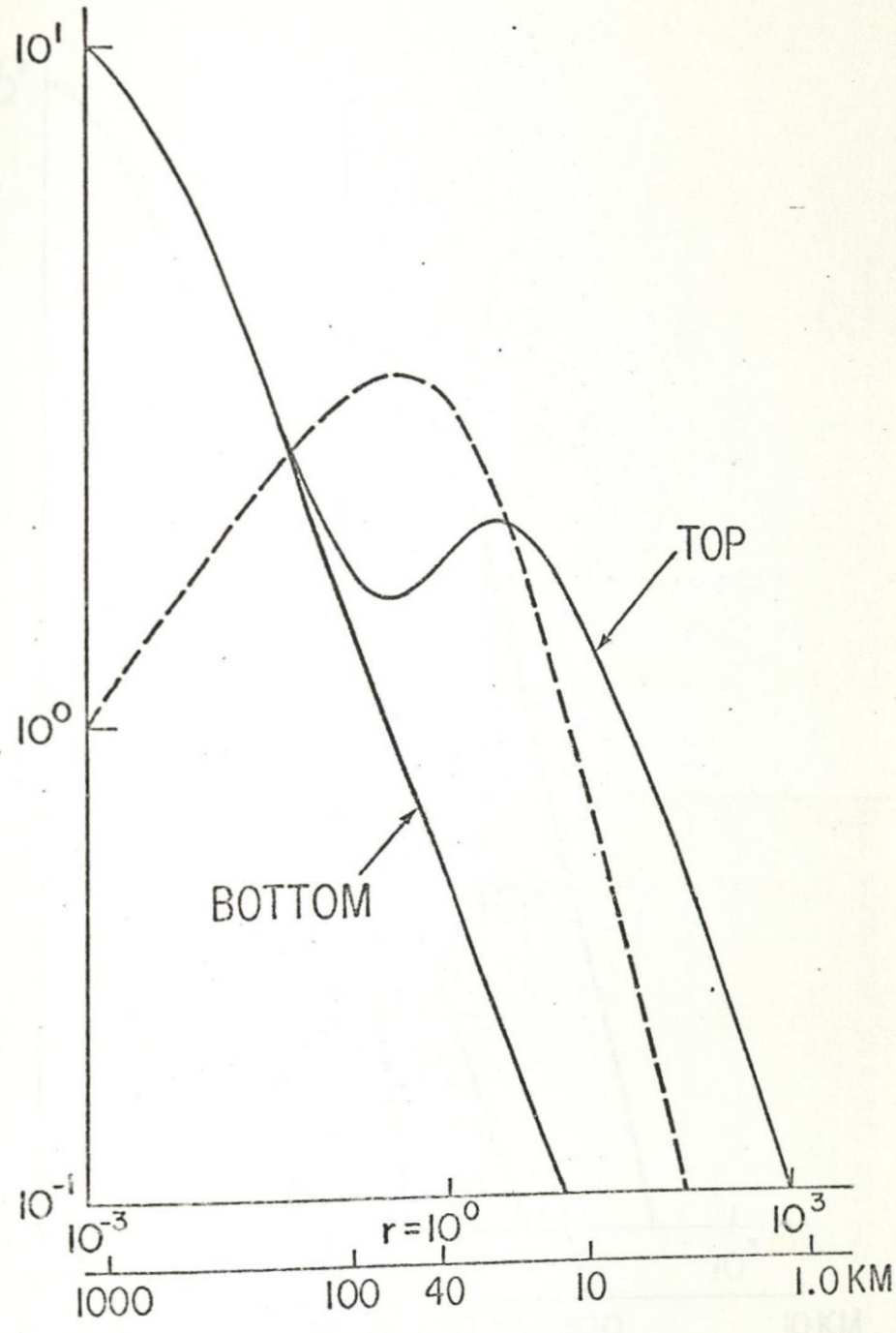
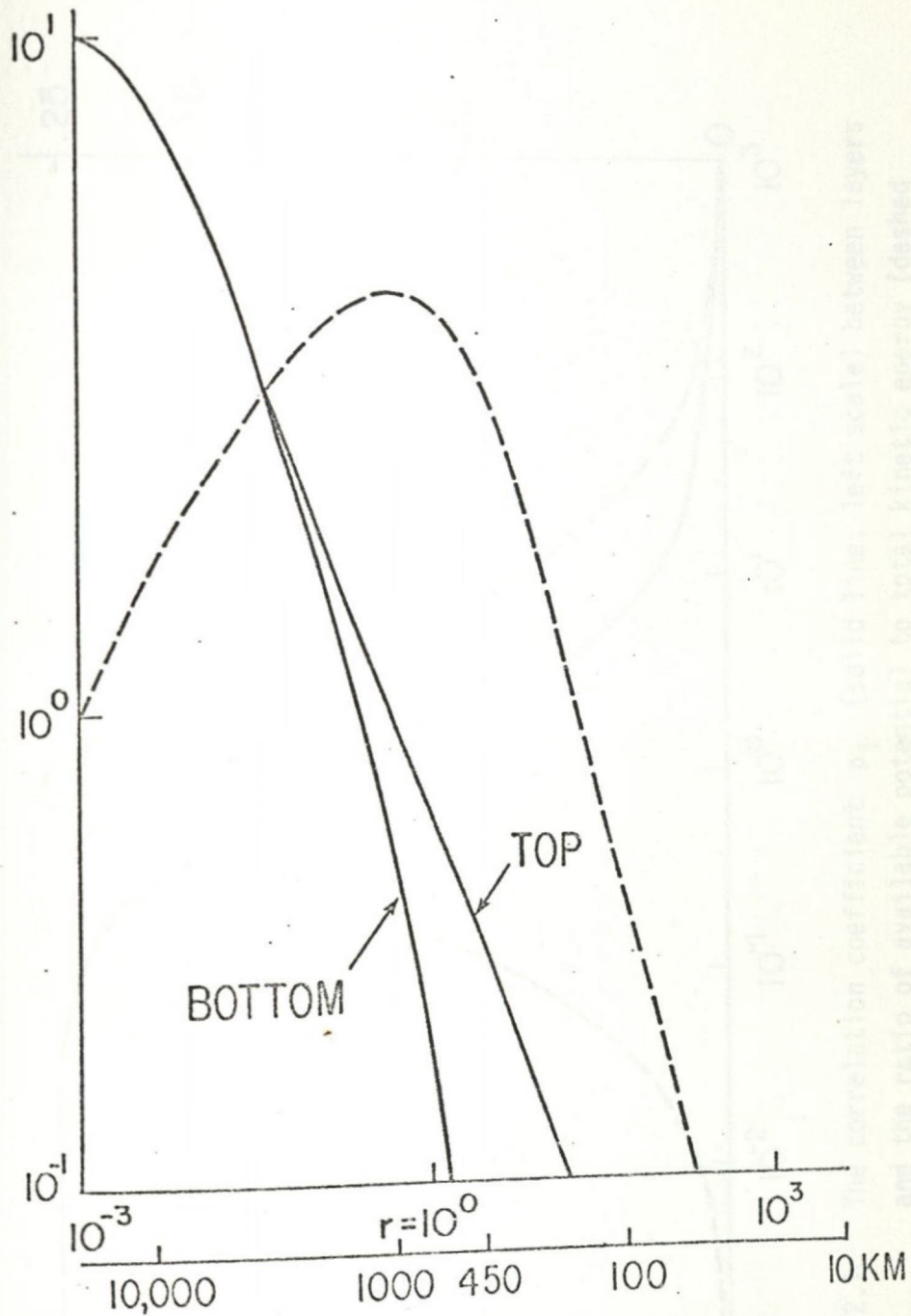Figure ... The kilometer ... in an atmosphere ... equal to 650 km.

Figure 2.1b The same as Fig. 2.1a except δ = 1. The kilometer
scale gives the inverse wavenumber in an atmosphere
with radius of deformation equal to 450 km.

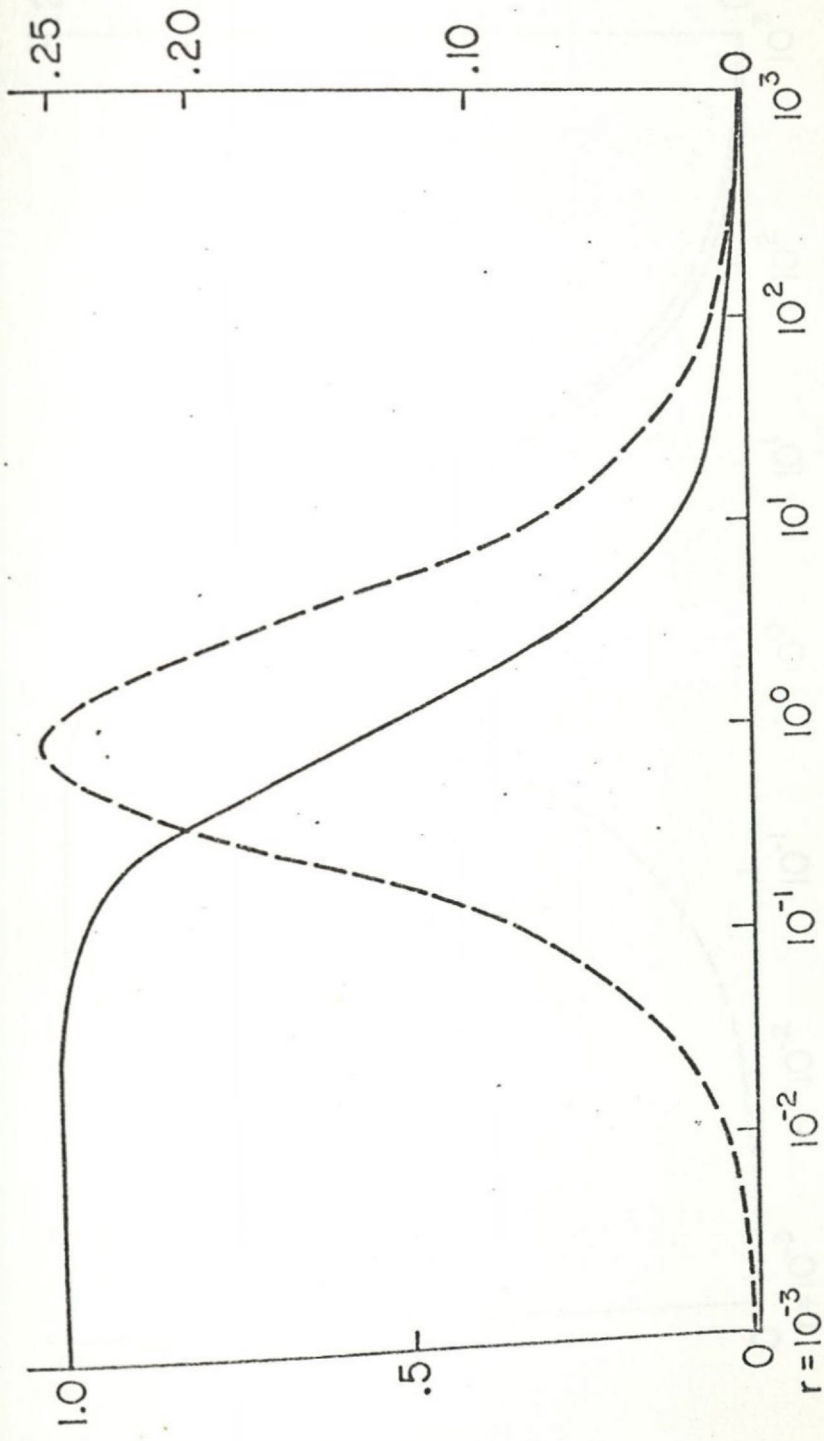Figure 2.1c The correlation coefficient ρ_i (solid line, left scale) between layers and the ratio of available potential to total kinetic energy (dashed line, right scale) for the case of (a).
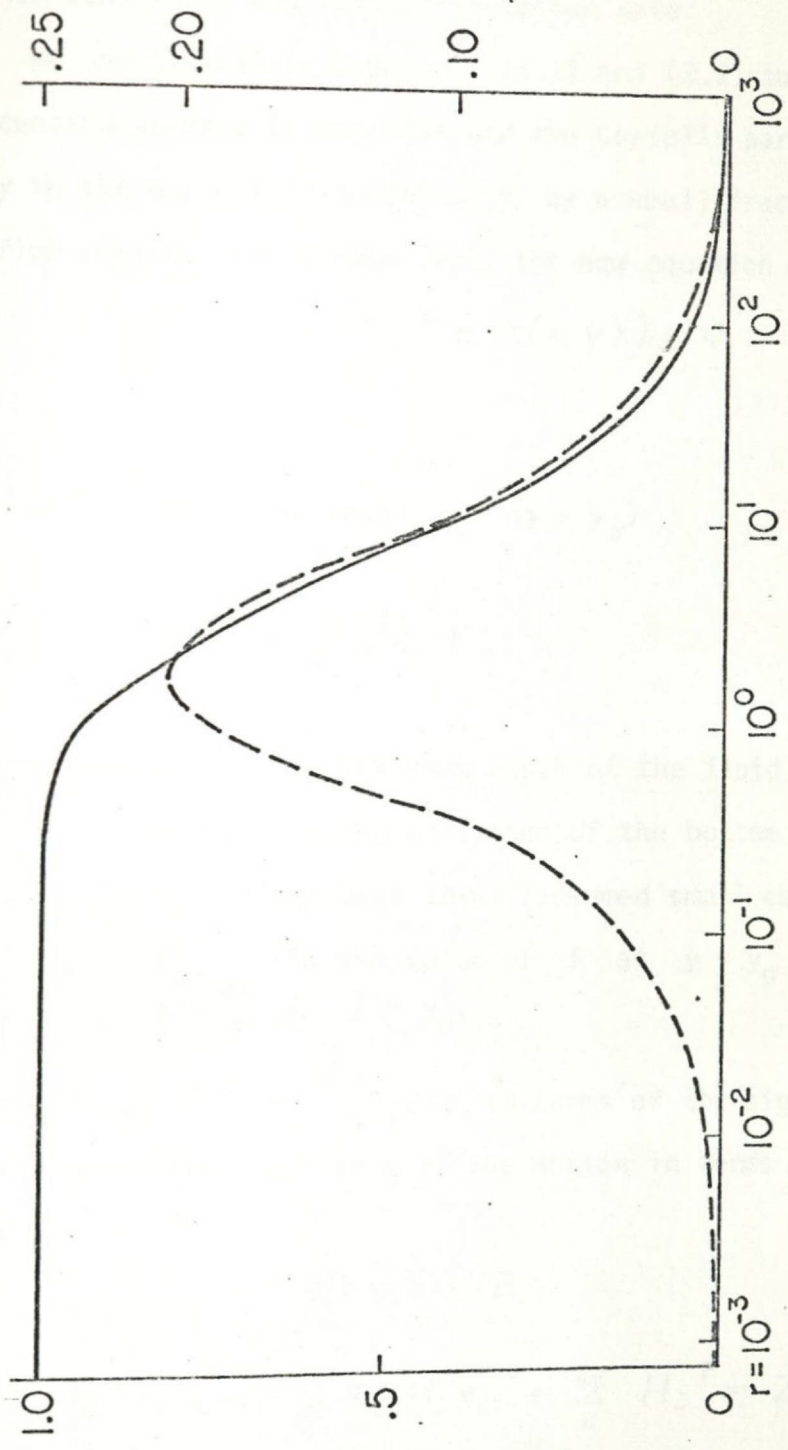
Figure 2.1d   The same as Fig. 2.1c except $\delta = 1$.

4. Bottom Topography and Variable Rotation Rate

We now generalize equations (2.1) and (2.2) to cases where the lower bounding surface is not flat and the Coriolis parameter f varies linearly in the northward direction y by a small fraction of itself in the flow region. For system (2.1) the new equation of motion is

$$\frac{\partial \zeta}{\partial t} + J(\psi, \zeta + H(x,y)) = 0 \tag{2.35}$$

where

$$H(x,y) = h(x,y) + \beta^* (y - y_o)$$

and

$$h(x,y) = \frac{f_o}{D} d(x,y) \quad .$$

Here,

D   is the mean depth of the fluid

$d(x,y)$ is the elevation of the bottom above its average level (assumed small compared to D)

f_o is the value of f at $y = y_o$

$\beta^* = \frac{df}{dy}$ at $y = y_o$.

Expanding $H(x,y) = \sum_i H_i \phi_i(x,y)$ in terms of the eigenfunctions we may again express the invariants of the motion in terms of the general coefficients:

$$\sum_i x_i^2 = E \tag{2.36}$$

$$\sum_i k_i^2 x_i^2 - 2 \sum_i k_i H_i x_i + \sum_i H_i^2 = Z$$

Methods similar to those used previously then give

$$\mathcal{P}_i(x_i) = \sqrt{\frac{\alpha + \beta k_i{}^2}{\pi}} \; e^{-(\alpha + \beta k_i{}^2)\left(x_i - \frac{\beta k_i H_i}{\alpha + \beta k_i{}^2}\right)^2} \qquad (2.37)$$

as a first approximation to the distribution of x_i. Again, α and β are constants determined by E and Z subject to the conditions that $\alpha + \beta k_i{}^2 > 0$ for every i.

The distribution (2.37) has the same form as for flat-bottom flow ($H_i = 0$) except that the Guassian curve is centered on

$$\langle x_i \rangle = \frac{\beta k_i H_i}{\alpha + \beta k_i{}^2} \qquad (2.38)$$

instead of zero. Thus the average streamfunction field is an energy-weighted version of the topographic field. If the flow contains arbitrarily small scales of motinon then $\beta > 0$ and the correlation between streamfunction and topography is positive at all wavenumbers (anticyclonic flow over seamounts, vorticity decreasing northward). If $\beta < 0$ then the correlation is negative at all wavenumbers. Again the latter states are the relaxation states for fluids in which the energy is initially peaked near k_{max}. For all $\beta \neq 0$ the energy is enhanced on topographic scales:

$$\langle x_i{}^2 \rangle = \frac{1}{2} \frac{1}{\alpha + \beta k_i{}^2} + \frac{\beta^2 k_i{}^2 H_i{}^2}{(\alpha + \beta k_i{}^2)^2} \qquad (2.39)$$

In strongly damped numerical simulations of (2.35) Holloway and Hendershott (1974) report a positive correlation between topography

and streamfunction and a topographic enhancement of the energy
spectrum similar to (2.39) .

As a special case consider the situation with $h(x,y) = 0$,
$\beta^* \neq 0$ on $0 < x,y < L$ with $y_0 = L/2$. With $\beta > 0$ the mean
equilibrium flow is a broad westward-flowing interior current with
eastward return flow occurring near the north and south boundaries.

In the two-layer system, the effects of topography and vari-
able rotation rate are non-equivalent in the sense that topography
alters the expression for potential vorticity in the lower layer only.
The governing equations are (2.2) with

$$\mathcal{S}_1 = \nabla^2 \psi_1 + F_1(\psi_2 - \psi_1) + \beta^*(y - y_0)$$

$$\mathcal{S}_2 = \nabla^2 \psi_2 + F_2(\psi_1 - \psi_2) + \beta^*(y - y_0) + h$$

Let $\quad h = \sum_i h_i \varphi_i \quad$ and $\quad \beta^*(y-y_0) = \sum_i h_i^* \varphi_i \quad$. Then the
joint distribution of a_i, b_i is given by:

$$P_i(a_i, b_i) = \frac{\sqrt{Q_i R_i - P_i^2}}{\pi} \exp\left[-Q_i(a_i - a_i^0)^2 \right. \tag{2.40}$$
$$\left. - R_i(b_i - b_i^0)^2 + 2P_i(a_i - a_i^0)(b_i - b_i^0)\right]$$

where Q_i, R_i, P_i are again given after (2.29) and

$$a_i^0 = a_i^h + a_i^*$$

$$b_i^0 = b_i^h + b_i^*$$

where

$$a_i^h = \frac{\beta_1 \beta_2}{F_2 \delta} \frac{r(r+1+\delta)}{(QR-P^2)} h_i$$

$$b_i^h = \frac{\beta_2}{F_2 \delta} \frac{r(r+1+\delta)}{(QR-P^2)} [\alpha + \beta_1(r+1)] h_i$$

$$a_i^* = \frac{\beta_1}{\delta F_1} \frac{r(r+1+\delta)}{(QR-P^2)} \left[\alpha + \frac{\beta_2}{\delta}(r+1+\delta)\right] h_i^*$$

$$b_i^* = \frac{\beta_2}{\delta F_2} \frac{r(r+1+\delta)}{(QR-P^2)} [\alpha + \beta_1(r+1+\delta)] h_i^*$$

The new expectation values are

$$\langle a_i \rangle = a_i^0$$

$$\langle a_i^2 \rangle = \frac{R_i}{2(Q_i R_i - P_i^2)} + (a_i^0)^2$$

and similarly for $\langle b_i \rangle$, $\langle b_i^2 \rangle$, $\langle a_i b_i \rangle$. The average flow field con-
sists of a topographic part and a β^* -part. The ratio of upper to
lower mean topographic flow is

$$\frac{\beta_1}{\alpha + \beta_1(r+1)}$$

which, for large $\left|\frac{\beta_1}{\alpha}\right|$, (red kinetic energy spectra), is nearly unity
for $r \ll 1$ and decreases sharply at $r = 1$. Thus bottom topography

affects the equilibrium upper layer flow only at scales large compared
to the radius of deformation. Smaller scale topography traps energy
preferentially in the lower layer. For large

$$\left|\frac{\beta_1}{\alpha}\right| \, , \, \left|\frac{\beta_2}{\alpha}\right|$$

the ratio a_i^*/b_i^* is nearly unity and both layers are equally
affected by the variable rotation rate.

5. Numerical Verification

To test our theory we have developed a numerical model that solves the equations (2.2) for flat-bottom two-layer flow in spectral form. The model ocean is a square box in which the streamfunctions are represented

$$\Psi = \sum_{n=1}^{K} \sum_{m=1}^{K} \Psi_{nm} \sin \frac{n\pi x}{L_{box}} \sin \frac{m\pi y}{L_{box}}$$

with $K = 31$ in the cases discussed. The average layer dpeths stand in the ratio $\delta = 1/7$. Our computer program implements the fast method of Orszag (1971) in which the derivatives are calculated in Fourier space and then transformed to physical space where the Jacobian is formed at discrete points and then inverse-transformed. This algorithm is <u>exactly equivalent</u> to, although computationally much faster than the direct spectral convolution written in equation (2.6). Our time steps are center-differenced with periodic smoothing to remove the computational mode.

In two experiments (summarized in Table 2.1) we have stepped the model equations forward from arbitrarily chosen initial states under inviscid conditions. We have also solved the equations (2.31) iteratively for the inverse temperatures α, β_1, β_2 corresponding to the initial states and then computed from equations (2.32) the final statistical states toward which the simulations should relax if our theory is correct. In Figures (2.2 - 2.5) the predicted final states are drawn with dashed lines. For reasons both aesthetic and practical,

83

TABLE 2.1

Summary of Numerical Experiments

Experiment	A	B
Initial conditions	layers correlated $\psi_2 \approx .5\psi_1$	uncorrelated spectral spike at $k = 8$
L_{box}	2200 km	1500 km
Radius of deformation	40 km	40 km
k_{def}	17.5	11.9
Length of experiment	800 days	500 days
RMS velocities top/bottom in cm per sec		
initial	10.00/5.00	13.03/4.11
after 2 mos	9.68/4.96	14.55/4.98
at end of experiment	10.07/5.38	13.86/5.66
predicted equilibrium	12.70/7.31	13.15/7.41
Available Potential energy in 10^6 erg per sq cm		
initial	8.62	8.29
after 2 mos	8.79	6.32
end	7.43	4.67
predicted	2.12	1.56

the model output data has been doctored in the innocuous manner described in Appendix C where the term "pseudospectrum" is also defined. Here we only note that the method of data reduction should not affect the comparison between theory and experiment.

In both experiments the model statistics generally evolve toward the predicted final states, although the two differ significantly even after several years of simulated time. The adjustment of the energy spectra is especially slow. However, many signatures of the predicted equilibrium state appear very early in the simulations and persist despite the fact that vigorous energy exchange between the different scales of motion is still occurring. In experiment A the layers are initially perfectly correlated with $\psi_2 = .5\,\psi_1$ plus a tiny perturbation and the initial kinetic energy spectra are bluer than the anticipated final spectra (Fig. 2.2). After two months the correlation between the layers has dropped significantly at the higher wavenumbers (Fig. 2.3a) and the kinetic energy spectra have steepened (Fig. 2.2a) for $k < 31$. In the same period the ratio of available potential to total kinetic energy evolves rapidly (Fig. 2.4). A puzzling aspect of the initial development is the relative slowness with which the highest wavenumbers ($k > 31$) equilibrate. Perhaps this is because these wavenumbers correspond to the corners of the box ($n \leqslant 31$, $m \leqslant 31$) in wavenumber space, and, by accident of this choice of wavenumber truncation, enter into relatively few triads. For the remainder of experiment A the statistical adjustment is slower but generally in the direction of the predicted final state. The kinetic

energy spectra converge at low wavenumbers (Fig. 2.2b) and the highest wavenumbers gradually relax toward the theoretical curves.

At the start of experiment B the layers are uncorrelated at all wavenumbers and the energy is concentrated in a spectral spike at $k = 8$. This experiment shows rapid development, probably because energy is initially baroclinic. Within two months 25% of the available potential energy has disappeared and the lowest wavenumbers show a significant positive correlation (Fig. 2.5a). Medium wavenumbers show a negative correlation which is probably associated with the strong conversion of potential to kinetic energy. After 140 days the negative correlation disappears. The final correlation curve is extremely close to that predicted by theory (Fig. 2.5b).
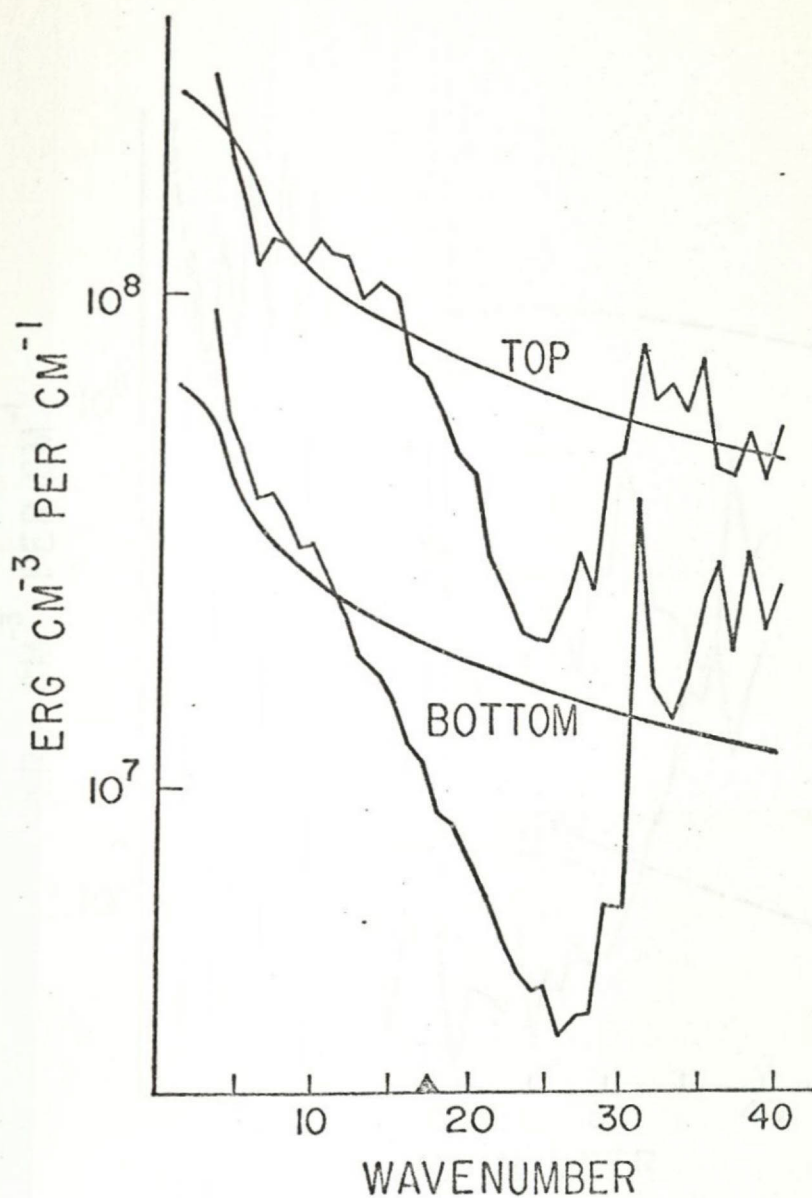
Figure 2.2a Pseudospectra of kinetic energy per unit volume in the top and bottom layers at the beginning of experiment A (smooth curves) and after 57 days. The black triangle on the abscissa marks the wavenumber corresponding to the radius of deformation.
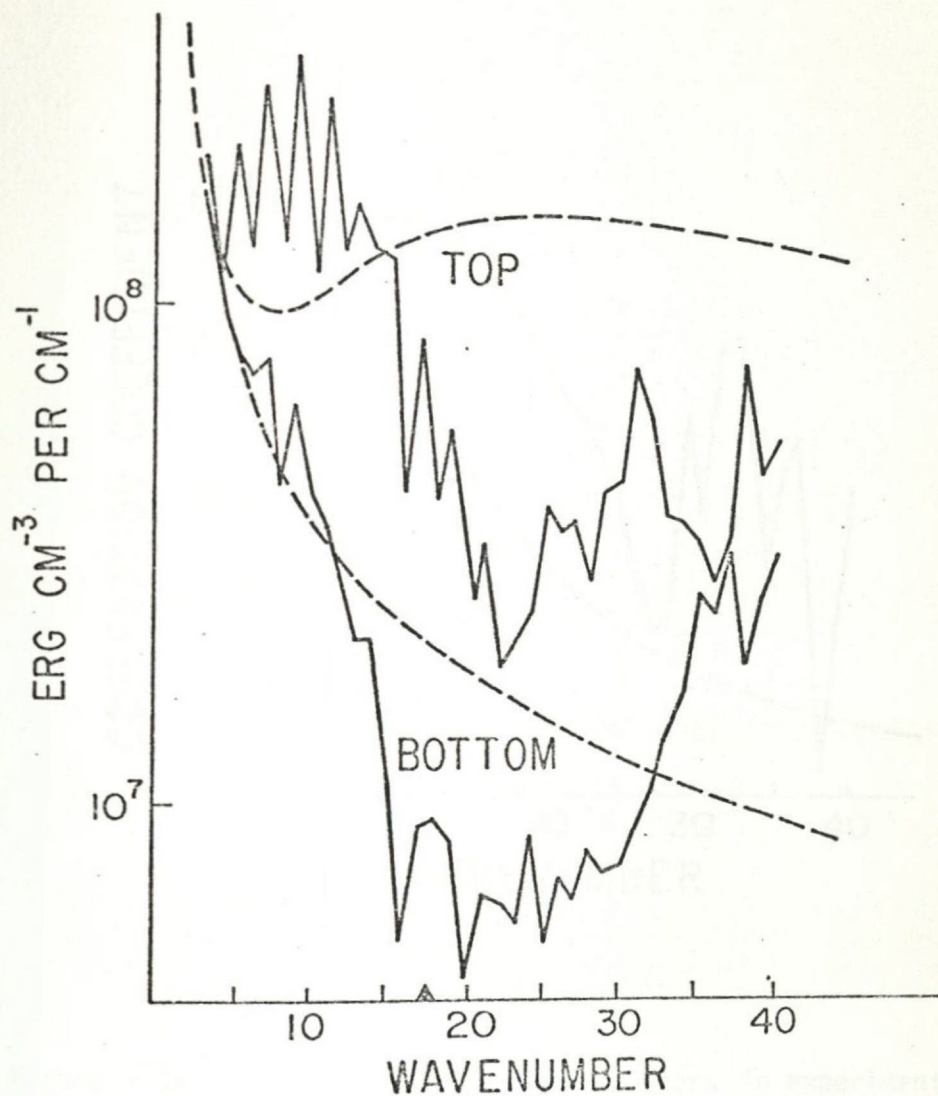
Figure 2.2b   Pseudospectra of kinetic energy per unit volume in experiment A after 794 days (solid lines) and the theoretical equilibrium state (dashed lines).
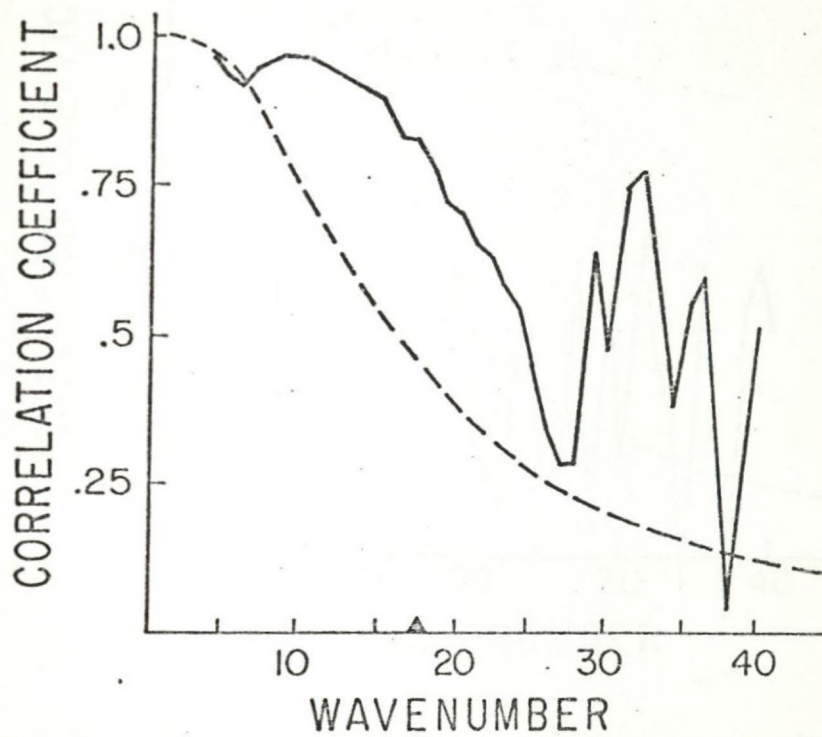
Figure 2.3a The correlation between layers in experiment A
after 57 days (solid curve) and the theoretical
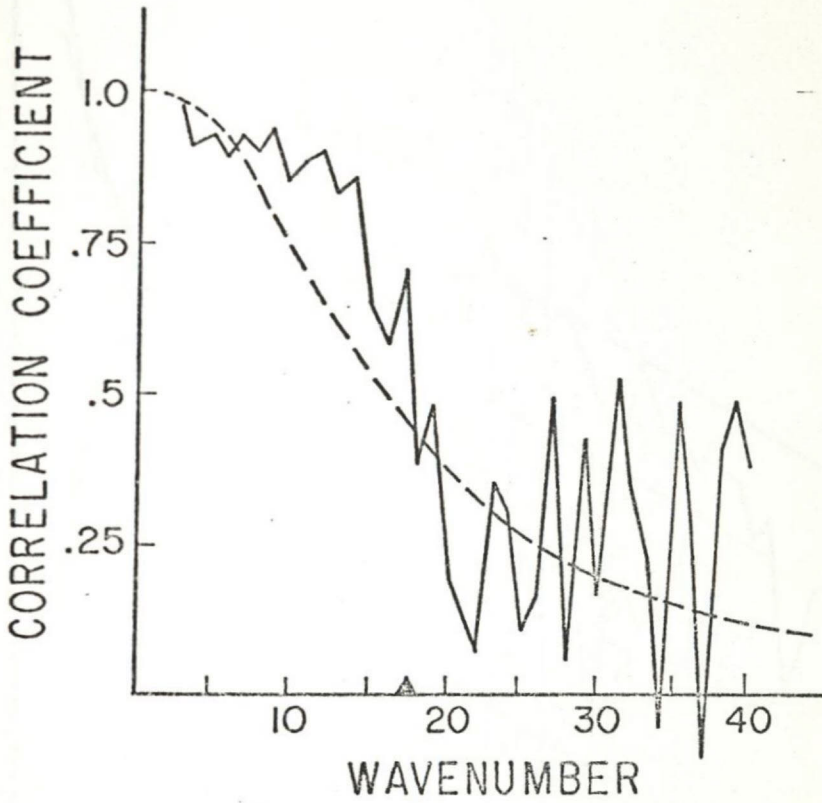equilibrium correlation (dashed curve).

Figure 2.3b   The correlation between layers in experiment A
after 794 days (solid curve) and the theoretical
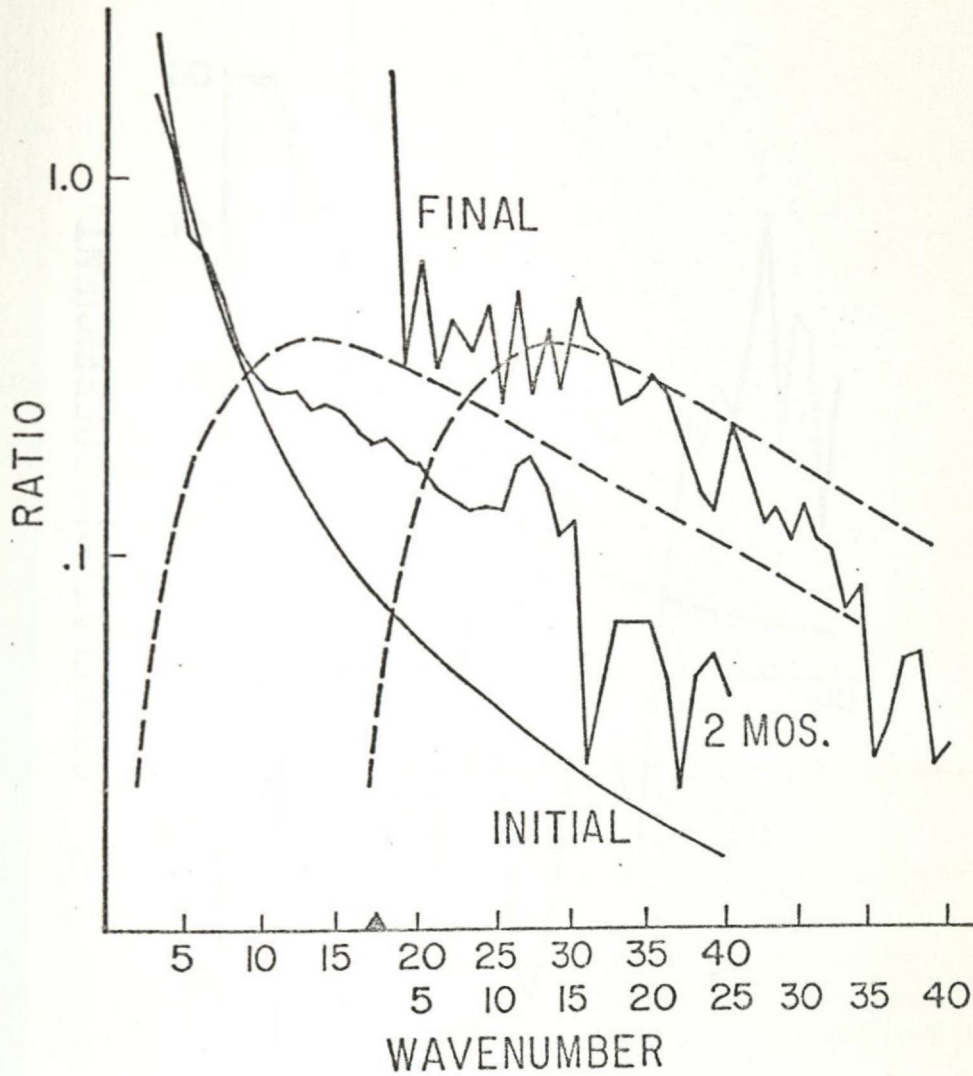equilibrium correlation (dashed curve).

Figure 2.4   The ratio of available potential to total kinetic energy in experiment A.   The theoretical equilibrium is represented by dashed curves.   Two of the curves have been displaced to the right.
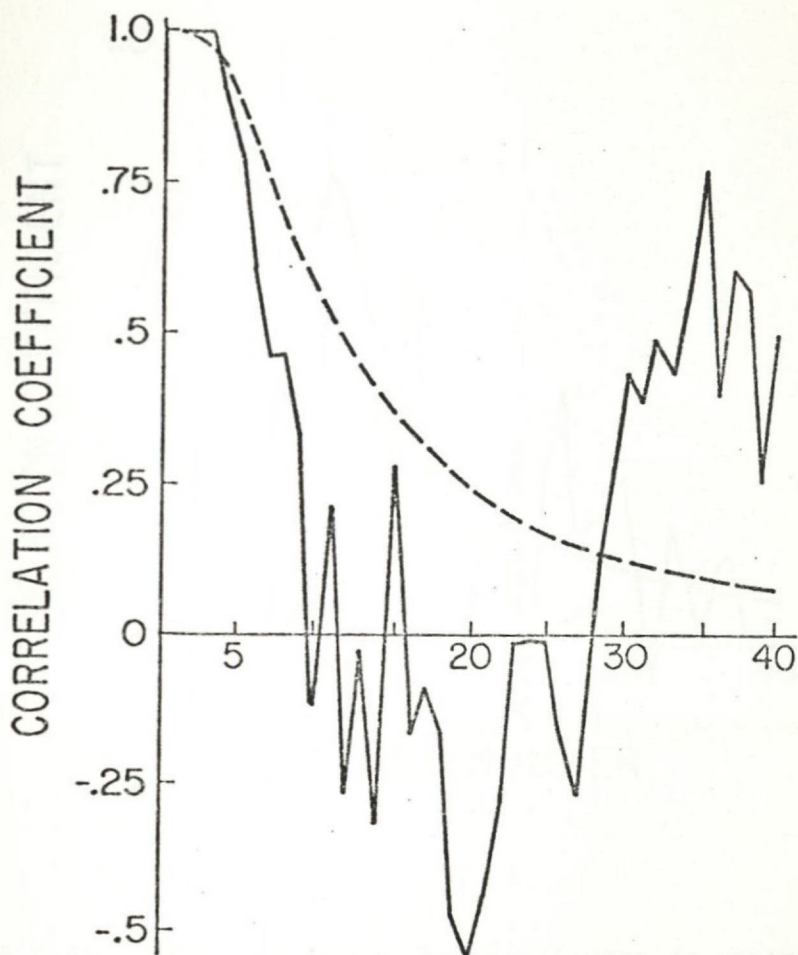
Figure 2.5a   The correlation between layers in experiment B
after 53 days (solid curve) and the theoretical
equilibrium correlation (dashed curve).   In
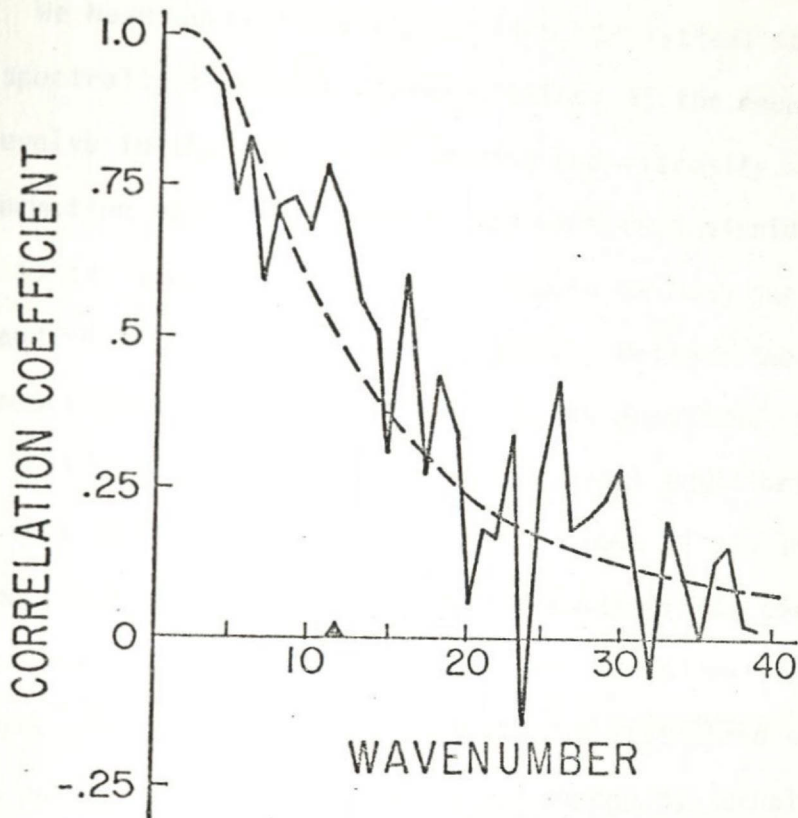experiment B the layers were initially uncorrelated.

Figure 2.5b   The correlation between layers in experiment B
after 498 days (solid curve) and the theoretical
equilibrium correlation (dashed curve).

6. Discussion

We have derived the equilibrium statistical states toward which spectrally-truncated representations of the equations of motion would evolve in the absence of forcing and viscosity. The theory gives no information about the speed of approach to inviscid equilibrium, which, as our experiments show, may depend on both the initial conditions and the statistic being considered. Neither the theory nor the experiments thus far performed address the question: to what extent do the real geophysical fluids resemble ideal equilibrium? We anticipate that waves (which occur in our systems if topography or variable rotation is present) will complicate the adjustment toward equilibrium. Numerical experiment by Rhines (1975) and by Holloway (in preparation) have shown that on scales where the Rossby wave phase speed approaches the rms particle speed the transfer of energy by turbulent interactions is inhibited.

It is of great interest to inquire whether the foregoing analysis can be extended to cases in which the forcing and damping are nonzero. We are pursuing this possibility. However, on the basis of current understanding, there is some cause for pessimism. Equilibrium statistical mechanics is incapable of yielding statistics at a time lag and such statistics are an important ingredient in nearly all turbulent closure approximations.

REFERENCES

Basdevant, C. and R. Sadourny, 1975: Ergodic properties of inviscid truncated models of two-dimensional incompressible flows. J. Fluid Mech., 69, 673.

Fox, D. G. and S. A. Orszag, 1973: Inviscid dynamics of two-dimensional turbulence. Phys. Fluids, 16, 169.

Holloway, G. and M. C. Hendershott, 1974: The effect of bottom relief on barotropic eddy fields. MODE Hot Line News No. 65.

Khinchin, A. I., Mathematical Foundations of Statistical Mechanics. Dover, 1949.

Kraichnan, R. H., 1967: Inertial ranges in two-dimensional turbulence. Phys. Fluids, 10, 1417.

Kraichnan, R. H., 1975: Statistical dynamics of two-dimensional flow. J. Fluid Mech., 67, 155.

Onsager, L., 1949: Statistical hydrodynamics. Nuovo Cim. Suppl. 9, 6, 279.

Orszag, S. A., 1971: Numerical simulation of incompressible flows within boundaries. Stud. Appl. Math., 50, 293.

Pedlosky, J., 1970: Finite amplitude baroclinic waves. J. Atmos. Sci., 27, 15.

Phillips, N. A., 1956: The general circulation of the atmosphere: a numerical experiment. Q. J. Roy. Met. Soc., 82, 123.

Rhines, P., 1975: Waves and turbulence on a beta-plane. J. Fluid. Mech., 69, 417.

This appendix proves (2.13) and the assertion about (2.14).
Suppose $m = 2$. By definition,

$$\Omega(E, Z) = \lim_{\delta E, \delta Z \to 0} \frac{1}{\delta E \cdot \delta Z} \iiint_{\substack{E - \delta E/2 < E' < E + \delta E/2 \\ Z - \delta Z/2 < Z' < Z + \delta Z/2}} dv' \quad .$$

$$= \lim_{\delta E, \delta Z \to 0} \iiint_{\substack{0 < E_1 < E + \delta E/2 \\ 0 < Z_1 < Z + \delta Z/2}} dv_1 \cdot \left\{ \frac{1}{\delta E \cdot \delta Z} \iiint_{\substack{E - E_1 - \delta E/2 < E_2 < E - E_1 + \frac{\delta E}{2} \\ Z - Z_1 - \delta Z/2 < Z_2 < Z - Z_1 + \frac{\delta Z}{2}}} dv_2 \right\}$$

$$= \iiint_{\substack{0 < E_1 < E \\ 0 < Z_1 < Z}} dv_1 \, \Omega_2(E - E_1, Z - Z_1)$$

$$= \int_0^E dE_1 \int_0^Z dZ_1 \left[\Omega_1(E_1, Z_1) \, \Omega_2(E - E_1, Z - Z_1) \right]$$

The upper integration limits may be made infinite because
$\Omega_2(E - E_1, Z - Z_1)$ is zero for $E_1 > E$ or $Z_1 > Z$. The extension
to $m > 2$ is straightforward.

Now let $\Gamma = \Gamma_1 + \Gamma_2$ and let M_1 be a region of the
subspace Γ_1, in which $(x_1, x_2, \ldots, x_r)$ serve as Cartesian coordin-
ates. Let M be the region of Γ such that for every $P \in M$ the

first r coordinates of P represent a point $P_1 \in M_1$. Let f(P) be a phase function defined on $P \in \Gamma$ with the falues:

$$f(P) = \begin{cases} 1 & \text{if } P \in M \\ \\ 0 & \text{otherwise} \end{cases}$$

Now, according to (   ) the probability that $P_1 \in M_1$ is equal to:

$$\mathcal{P}(P_1 \in M_1) = \mathcal{P}(P \in M)$$

$$= \lim_{\delta E, \delta Z \to 0} \frac{1}{\Omega(E,Z)} \frac{1}{\delta E \delta Z} \iiint f(P') dV'$$

$$E - \frac{\delta E}{2} < E' < E + \frac{\delta E}{2}$$
$$Z - \frac{\delta Z}{2} < Z' < Z + \frac{\delta Z}{2}$$

But

$$\lim \frac{1}{\delta E \cdot \delta Z} \iiint f(P') dV' \longrightarrow \iint_{\Gamma_1} f \, \Omega_2 (E - E_1, Z - Z_1) dV_1$$

because f depends only on the coordinates of Γ_1. Thus

$$\mathcal{P}(P_1 \in M_1) = \iint_{M_1} \frac{\Omega_2 (E - E_1, Z - Z_1)}{\Omega(E,Z)} dV_1$$

which proves (2.14).

This appendix shows that there exists a unique solution α, β to the equations

$$\frac{1}{2} \sum_i \frac{1}{\alpha + \beta k_i^2} = E \tag{2.B.1}$$

$$\frac{1}{2} \sum_i \frac{k_i^2}{\alpha + \beta k_i^2} = k_*^2 E$$

subject to the constraints $\alpha = \beta k_i^2 > 0$ for every i, provided that $k_{min}^2 < k_*^2 < k_{max}^2$.

The above equations are equivalent to:

$$\begin{cases} -\frac{\partial f}{\partial \alpha}(\alpha, \beta) = E \\ -\frac{\partial f}{\partial \beta}(\alpha, \beta) = k_*^2 E \end{cases}$$

where $f(\alpha, \beta) = \ln \phi(\alpha, \beta) = -1/2 \sum_i \ln(\alpha + \beta k_i^2) + \text{constants}$.
Thus $f(\alpha, \beta)$ is defined on the infinite sector $R_{\alpha\beta}$ of the α-β plane in which $\alpha + \beta k_i^2 > 0$ for every i. By direct computation, one can verify that on $R_{\alpha\beta}$:

$$\tag{2.B.2}$$

$$-f_\alpha > 0, \quad -f_\beta > 0 \quad \text{and} \quad (f_{\alpha\alpha})(f_{\beta\beta}) - (f_{\alpha\beta})^2 > 0 .$$

We can therefore define curvilinear coordinates on $R_{\alpha\beta}$ by:

$$\gamma = f_\beta / f_\alpha \qquad\qquad \delta = -f_\alpha .$$

In terms of the curvilinear coordinates, the region $R_{\alpha\beta}$ is described by:

$$K_{min}^2 < \gamma < k_{max}^2$$

$$0 < \delta < \infty$$

and the equations (2.B.1)

$$\begin{cases} \delta = E \\ \gamma = k_*^2 \end{cases}$$

which always has a unique solution in $R_{\alpha\beta}$ because, from (2.B.2):

$$\frac{\partial(\gamma,\delta)}{\partial(\alpha,\beta)} = \frac{f_{\alpha\alpha} f_{\beta\beta} - (f_{\alpha\beta})^2}{f_\alpha} < 0 \quad \text{throughout } R_{\alpha\beta}.$$

APPENDIX 2.C

In order to facilitate comparison of our model statistics with the theoretical curves in section 3 we have adopted the following method of analyzing the model output: We apply the standard statistical estimators for square amplitudes and correlations to groups of Fourier modes corresponding to wavenumber vectors $\vec{k} = (n,m)$ lying in circular bands of unit width in the n-m plane. This type of averaging is strictly correct only in the case of homogeneous isotropic flow where the Fourier amplitudes corresponding to different vectors of the same length can indeed be regarded as independent realizations of the same random variable. Let $N(k)$ be the number of modes contained in the band centered on integer wavenumber k in our truncated model. For an infinitely large box and perfect resolution of the flow, $N(k)$ is a jittery function of k. To remove the artificial jitters from our "pseudospectral" estimates we multiply each estimate by a smoothing factor

$$S(k) = \frac{C\,k}{N(k)}$$

where C is a constant obtained by least-squares fitting Ck to $N(k)$. The above averaging procedures were applied equivalently to the model output and the theoretically determined equilibrium state calculated from equations (2.32).